



UNIVERSITI
TEKNOLOGI
PETRONAS

FINAL YEAR PROJECT II: DISSERTATION

**SYNTHESIS AND CHARACTERIZATION OF MORPHOLOGY
DEPENDENT NICKEL OXIDE CATALYST TO AID
HYDRODEOXYGENATION OF PHENOL TO BIO-FUELS**

PREPARED BY:

HEMAVATHY RAJAN THIRAN
14994

SUPERVISOR:

DR SUJAN CHOWDHURY

Preliminary report submitted in partial fulfilment of the requirements for the
Bachelor of Engineering (Hons)
(Chemical Engineering)

Universiti Teknologi PETRONAS

Bandar Seri Iskandar

31750 Tronoh

Perak Darul Ridzuan

CERTIFICATION OF APPROVAL

SYNTHESIS AND CHARACTERIZATION OF MORPHOLOGY DEPENDENT NICKEL OXIDE CATALYST TO AID HYDRODEOXYGENATION OF PHENOL TO BIO-FUELS

By

HEMAVATHY RAJAN THIRAN

14994

A project dissertation submitted to the
Chemical Engineering Programme
Universiti Teknologi PETRONAS
in partial fulfilment of the requirement for the
BACHELOR OF ENGINEERING (Hons)
(CHEMICAL)

Approved by,

(_____)

UNIVERSITI TEKNOLOGI PETRONAS
TRONOH, PERAK

JANUARY 2015

CONTENTS

ABSTRACT	7
CHAPTER 1	8
INTRODUCTION	8
1.1 BACKGROUND OF STUDY	8
1.2 PROBLEM STATEMENT	10
1.3 OBJECTIVE AND SCOPE OF STUDY	11
CHAPTER 2	12
LITERATURE REVIEW AND THEORY	12
2.1 Nickel and nickel oxide	12
2.2 Hydrodeoxygenation	16
CHAPTER 3	19
METHODOLOGY AND PROJECT WORK.....	19
3.1 Materials and Equipment:	19
3.2 Procedures	22
3.3 Project Timeline	Error! Bookmark not defined.
3.4 Key milestone.....	23
CHAPTER 4	25
RESULTS	25
CHAPTER 5	54
CONCLUSION AND RECCOMENDATION	54
REFERENCES.....	55

LIST OF TABLES

Figure 1: “Total Primary Energy Supply by resource 1993, 2011 and 2013”	8
Figure 2: Transformation to produce biofuels	10
Figure 3: The biomass sources	10
Figure 4: XRD patterns of NiO prepared with different percentage of mass of water at the required calcined temperature.	14
Figure 5: Properties of bio-oil versus crude oil.....	16
Figure 6: Four main pathways of hydrodeoxygenation	17
Figure 7: The traditional hydrodeoxygenation method.....	18
Figure 8: Timelines for FYP I.....	23
Figure 9: Timelines for FYP II.....	23
Figure 10: Key milestone	24
Figure 11: The descending order of the base reactivity.	31
Figure 12: Different structures of nickel oxide catalyst using TEM.....	35
Figure 13: The diffraction rings of nickel oxide catalyst.....	38
Figure 14: EELS result.....	41
Figure 15: SEM result of 2M of KOH nickel oxide catalyst	42
Figure 16: SEM result of 0.125M of NaOH of nickel oxide catalyst	42
Figure 17: Raman result for 0.125M NaOH	43
Figure 18: Raman result for 4M NaOH	44
Figure 19: Raman result for 2M KOH	45
Figure 20: Raman result for 2M NaOH	46
Figure 21: Comparisons of RAMAN results of four bases.....	47
Figure 22: Graph of rate of reactivity versus pH values	51
Figure 23: The XRD pattern of the nickel oxide of 0.125M of NaOH.....	52
Figure 24: The XRD pattern of the nickel oxide of 2M of KOH.....	53

ABSTRACT

Various nickel oxide (NiO) nanostructures were prepared in different bases via hydrothermal method. The bases used in this research paper are sodium hydroxide, ammonia, potassium hydroxide and sodium carbonate. NiO nanoparticles, nanorods, nanohexagonal, nanocubic, nanopentagon and nanocuboid with different sizes were obtained. The obtained nanoparticles have been characterized by means of X-ray powder diffraction (XRD), scanning electron microscopy (SEM), transmission electron microscopy (TEM) and RAMAN. A possible growth mechanism is proposed including the formation of hierarchical microspheres aggregated from nuclei

CHAPTER 1

INTRODUCTION

1.1 BACKGROUND OF STUDY

Recently, the core concern in the energy problem is the running down of petroleum. So far, petroleum still takes control nearly one third of the entire world's energy wealth and it's one of the expensive sources of energy. The Figure 1 below is the "Total Primary Energy Supply by resource 1993, 2011 and 2013" and this pie chart is obtained from the "WEC Survey of Energy Resources 1995, World Energy Resources 2013 and WEC World Energy Scenarios to 2050". As you can see from the pie chart below from the year 1993 the consumption of fossil fuels has decreased by 6% and the renewables resources has increased by 5%. This shows that the demand of bio-oils are also increased which lies under the renewables segment

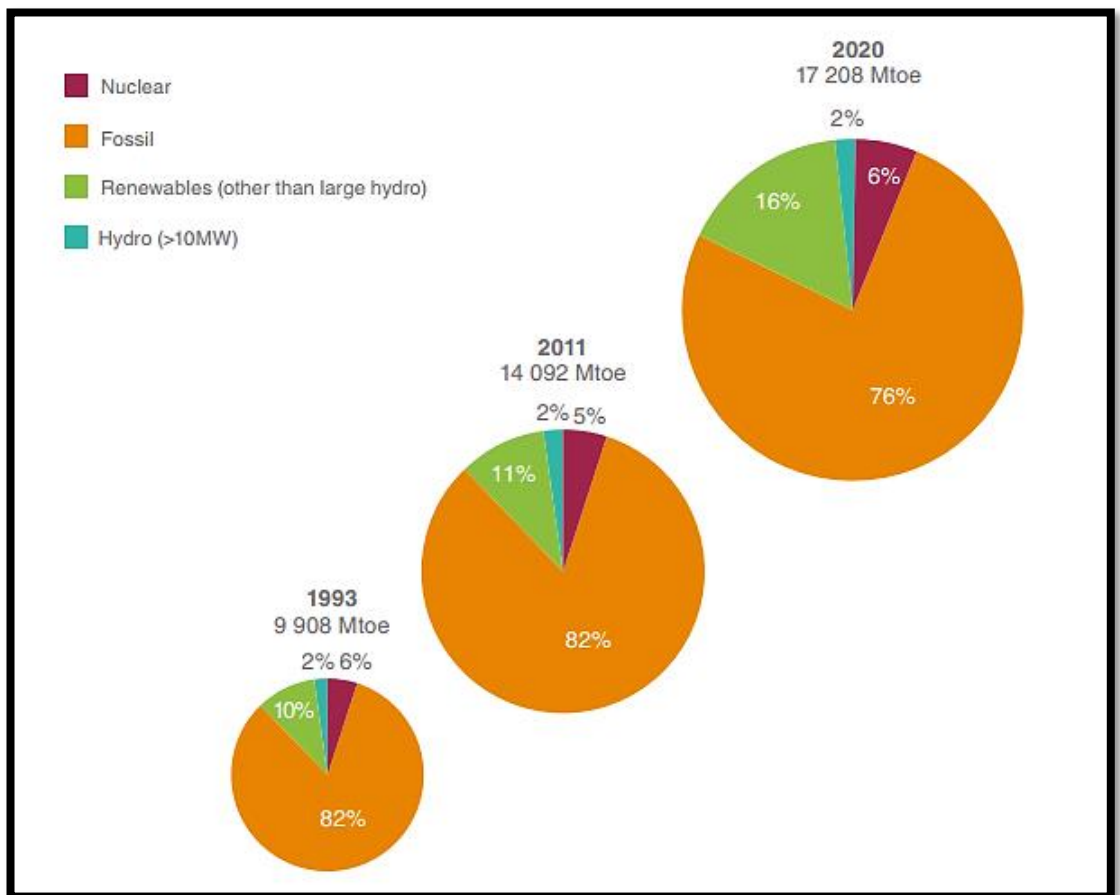


Figure 1: "Total Primary Energy Supply by resource 1993, 2011 and 2013"

In this research paper we are focusing on the hydrodeoxygenation of phenols in forming the biofuels. Generally, bio-oils are produced continuously from fast pyrolysis of ample biomass and have played a role as the feedstock of the renewable production of biofuels. Furthermore, it has magnetised the attention of the global. Presently, biofuels have been estimated to be a favourable substitute to fossil fuels.

In order to produce the biofuels we are using the method of hydrodeoxygenation the phenols. The definition of hydrodeoxygenation was taken from Wikipedia and it spells like “Hydrodeoxygenation (HDO) is a hydrogenolysis process for removing oxygen from oxygen containing compounds. It is of interest for biofuels, which are derived from oxygen-rich precursors like sugars”. This process works best with a catalyst such as nickel-molybdenum on gamma alumina but in this process we are using nickel. There are few reasons why this catalyst are chosen instead of others and are further discussed below.

Bio-oil produced from fast pyrolysis of lignocellulosic biomass is a promising alternative fuel to replace fossil fuels. Fast pyrolysis includes heating the biomass at elevated temperatures in the range of 400–550 °C in the absence of oxygen. Bio-oil may also be produced by slow pyrolysis, liquefaction or other alternative methods [1] .

By evading hydrogenation and cracking reactions, hydrogen can be used efficiently because of the great oxygen content of the bio-oils and the yearning for completely renewable fuel requirements.

Bio-oil has environmental advantages when compared to fossil fuels because, when combusted, bio-oil produces less pollution than fossil fuels, specifically, half the NO_x, negligible quantities of SO_x emissions, and it is considered to be CO₂ neutral. Bio-oil chemical properties vary with material utilized for its production or the conditions under which it is produced.

1.2 PROBLEM STATEMENT

Malaysia produces plenty of bio-mass from sewage, municipal solid waste, agricultural crops & residues, industrial residues, forestry crops & residues, animal residues and lastly industrial residues as shown in the Figure 3 below and it has been extracted from the Biomass Innovation Centre. People are still not realising the benefits of bio mass and how valuable it is. As mentioned earlier everyone knows how important fuel is to run the world but like a coin which has two sides, tail and head, fuel has its own drawbacks. Fuel is one of the most expensive resources and it is predicted that fuel might be depleting in a few decades. Besides, fuel also generates a lot of environmental problems. Our purpose is to prepare something which is efficient and useful which is the biofuels. Below, Figure 2 shows the transformation taken to produce biofuels.

BIOMASS → BIO-OILS → BIOFUELS

Figure 2: Transformation to produce biofuels

We're also using the nickel and iron as a catalyst because it is cheaper and effective.

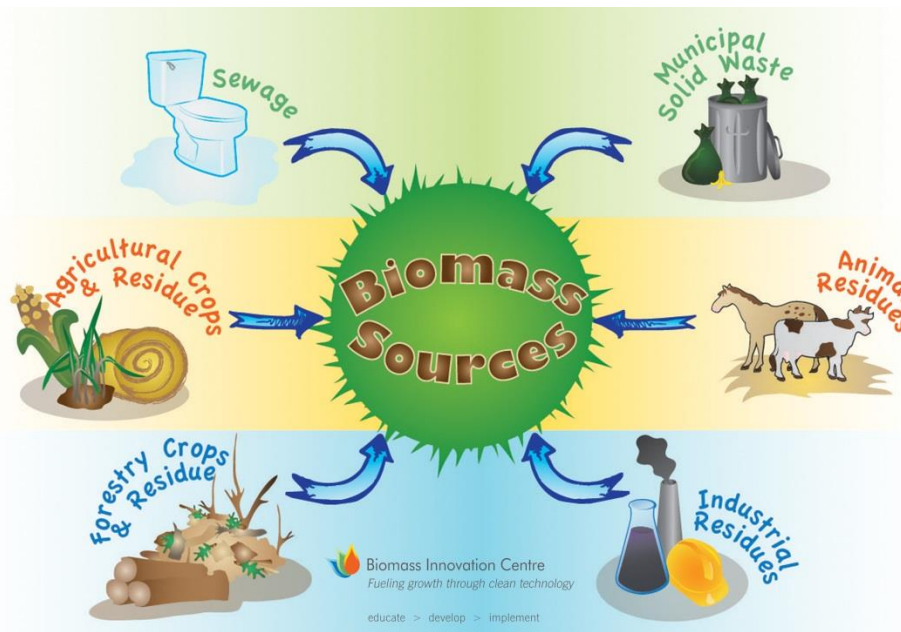


Figure 3: The biomass sources

1.3 OBJECTIVE AND SCOPE OF STUDY

The objectives of the project are as follows:

- ✚ To produce different structure of nickel oxide.
- ✚ To produce a cheaper catalyst which nickel oxide for bio-oil conversion.
- ✚ To produce a catalyst which is efficient and which is stable for a long period of time.
- ✚ To enhance the production of biofuels.
- ✚ To choose the best base for the nickel oxide catalyst.

The scopes of study covered for this project include:

- ✚ Synthesising different structures of nickel oxide.
- ✚ Synthesising a cheaper catalyst which Fe is doped to nickel oxide bio-oil conversion.
- ✚ Synthesising a catalyst which is efficient and stable for a long period of time.
- ✚ Enhance the production of biofuels

CHAPTER 2

LITERATURE REVIEW AND THEORY

2.1 Nickel and nickel oxide

Nickel is a white-silver solid, flexible, and malleable metallic element. This element reduces the rust propagation rate and capable of achieving a high polish that is used mostly in alloys and as an accelerator [2] [3]. Nickel is an organic element with atomic number of 28, with a representation Ni and fits to the transition metal group. Unalloyed nickel are powdered to capitalize on the bare surface area to prove a momentous chemical reaction because greater fragments of the element are not quick to respond with air at ambient situations due to the development of a shielding oxide exterior.

The main reason nickel is used for this experiment is to yield a higher production that is achieved with the catalytic pyrolysis for the first part of this research paper. As mentioned earlier in the previous paragraph, nickel is a transition metal and there are many other transition metals such as mercury, cerium, cobalt and titanium. The other reason nickel is chosen is because it is easier to be synthesized and less in cost compared to the others. Furthermore, this useful element minimizes life cycle expenses, has a very high stability and escalated the recyclability. Below shows the atomic dimensions and structure of nickel [3, 4].

Atomic Radius	149 pm
Covalent Radius	121 pm
Van der Waals Radius	163 pm
Crystal Structure	Face Centered
Lattice Angles	$\pi/2$, $\pi/2$, $\pi/2$
Lattice Constants	352.4, 352.4, 352.4 pm
Space Group Name	Fm ₃ m
Space Group Number	225

Table 1: Atomic dimensions and structure of nickel

Besides, compared to Platinum and Palladium catalysts, Nickel plays as a better attractive substitute this is because they are roughly three orders of degree less costly. As debated above, Nickel catalysts are vigorous for a large variety of synthesis in a hydrothermal situation together with HDN, HDS, gasification and HDO even though various catalysts are deficient in selectivity or stability.

In this era we should be providing a cost-economical, renewable, almost carbon-neutral method to yield hydrogen and fund to the growth of upgraded, long-lasting, cost-economical fuel cells. Besides some experimentalists discovered that nickel has become a recovered catalyst for processes when it is used in a high-pH atmosphere. They further discovered with their experimentalist colleagues that nickel's ability to produce hydrogen was significantly increased in an alkaline environment, a critical insight when considering whether a less expensive, nickel-based catalyst is a feasible alternative for the platinum catalysts used for hydrogen production from biomass. Peles and her team also confirmed the optimum size for the catalytic particles in fuel cells to ensure their effectiveness.

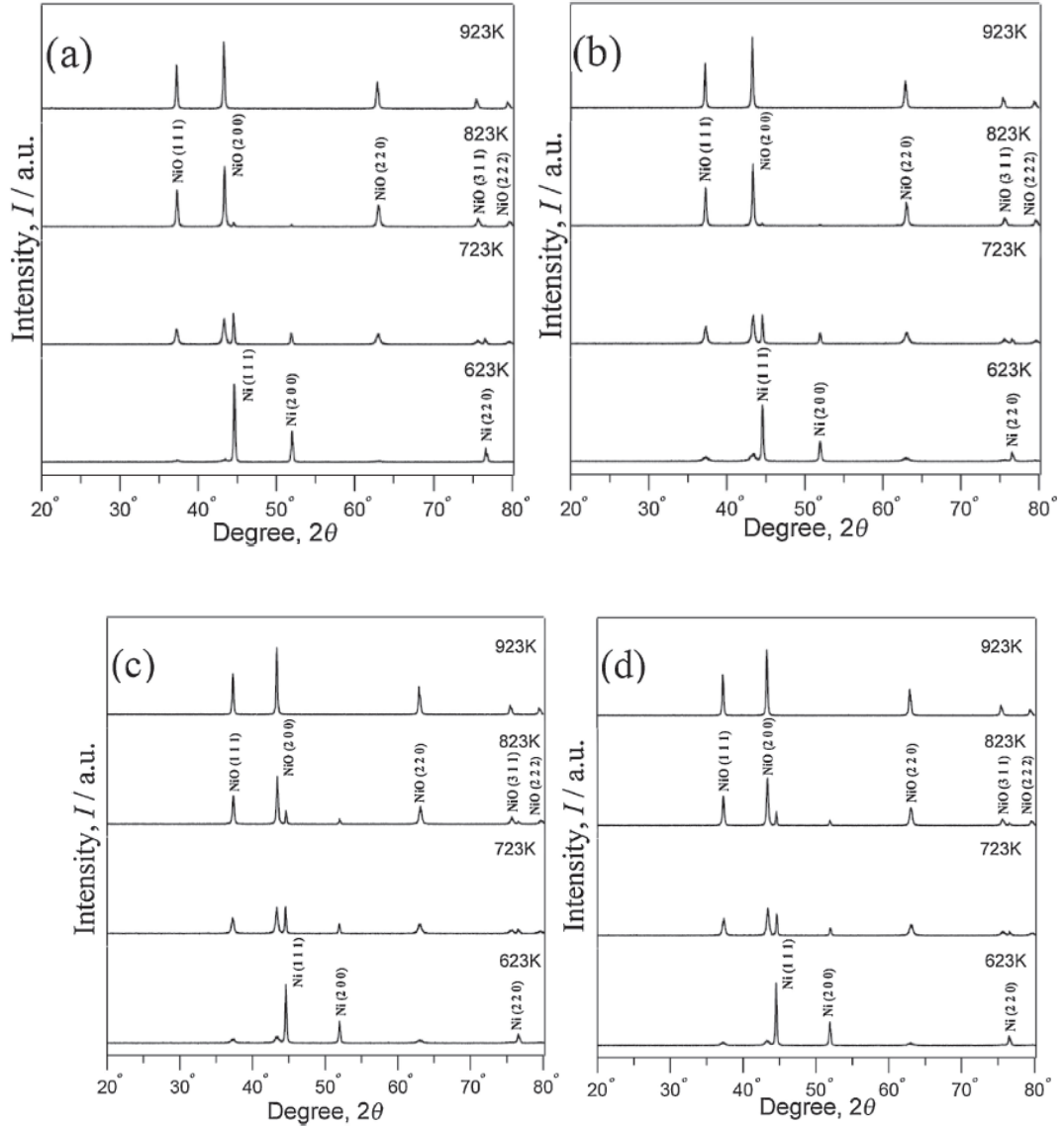


Figure 4: XRD patterns of NiO prepared with different percentage of mass of water at the required calcined temperature.

The figure above demonstrates the impact of temperature and water concentration on the physical characterizations of nickel oxide nanoparticles, from 623 to 923K for nearly three hours were carried out by XRD with altered quantities of water. At 623 K it is visible that only pure nickel nanoparticles are existed. It shows a usual Face-Centered Cubic (FCC) arrangement of nickel with three distinctive crests, labelled as the replications from {110}, {200} and {220} flat surface. By using copolymer as the surfactant, Surfactant-mediated techniques were carried out to prepare nickel nanoparticles.

Accordingly, the formation of Ni and NiO nanoparticles and their structural features were greatly dependent on the calcination temperature. With increasing calcination temperature, the intensities of the diffraction peaks of NiO increased, and the degree of crystallinity would be improved. To investigate the effects of H₂O on the synthesis, 10, 20 and 40 mass% H₂O were applied into the systems, and nanoparticles of Ni and NiO were obtained again.

Considering to the effects of H₂O concentration on the formation of NiO nanoparticles, the metallic Ni nanoparticles are presented with few amount of NiO at 623K (Fig. 3(a)). While H₂O concentration was increased at this calcination temperature (623 K), the diffraction peaks of NiO became more obviously, as shown in Figs. 3(b) 3(d). It is clear that by appropriate addition of H₂O, the phase and phase composition in the case of a mixed phase can be readily controlled. Similar trends of the influence of H₂O concentration could be found at 723 K.

2.2 Hydrodeoxygenation

Hydrodeoxygenation which is also known as HDO is a hydrogenolysis procedure designed for eliminating oxygen from oxygen comprising composites [9, 10]. It is derivated from oxygen-rich precursors like sugars and is mostly famous for biofuels. Besides, for the production of nylon-6 and nylon-66, catalytic hydrogenation of phenol is technically essential for the production of cyclohexanone and cyclohexanone.

The firmness and selectivity of catalysts persist as important encounters even when HDO is aided with a diversity of catalysts. This is because of the water existed within the bio-oil and also water formed from the HDO reaction. Usually at hydrotreating reactor temperatures approximately 400 °C the common supports catalyst such as γ -Al₂O₃ and SiO₂ damages and also oxidation of active metals present with the aid of water. Below shows the properties of bio-oil versus crude oil.

Composition	Bio-oil	Crude Oil
Water (wt %)	15–30	0.1
pH	2.8–3.8	-
density (kg/L)	1.05–1.25	0.86
viscosity 50 °C (cP)	40–100	180
HHV (MJ/kg)	16–19	44
C (wt %)	55–65	83-86
O (wt %)	28–40	<1
H (wt %)	5–7	11–14
S (wt %)	<0.05	<4
N (wt %)	<0.4	<1
Ash (wt %)	<0.2	0.1
H/C	0.9–1.5	1.5–2.0
O/C	0.3–0.5	≈0

Figure 5: Properties of bio-oil versus crude oil.

Usually, the hydrogenation of phenol is conducted out in the vapor stage with Pd catalysts but in this research we are using Fe doped with Ni. Great temperature is required because of vapour stage hydrogenation which usually causes the catalyst deactivation by coking during the process [11]. Liquid stage hydrogenation of phenol was done with Ni catalysts in a few studies. Nevertheless, to attain high phenol

conversions, high feed-back temperatures or elongated reaction time were still needed [10] [12].

In this paper we are focusing on the hydrodeoxygenation of phenol and this process is divided into 4 main pathways such as:

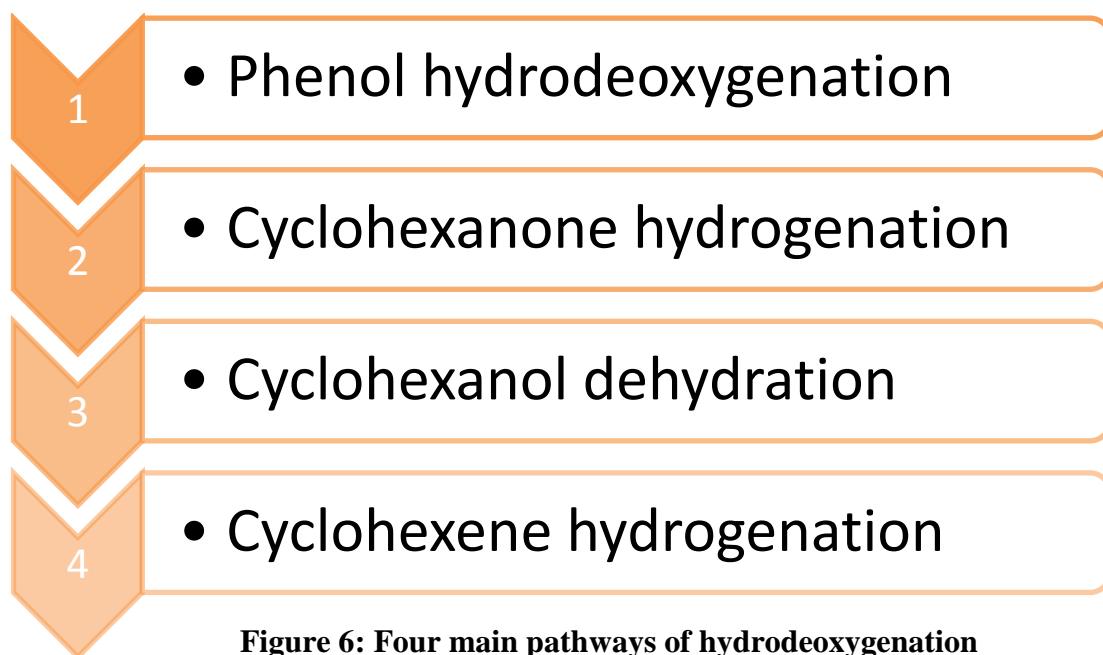


Figure 6: Four main pathways of hydrodeoxygenation

The diagram below shows the schematic diagram of a traditional hydrodeoxygenation pathway in a more detailed explanation visually.

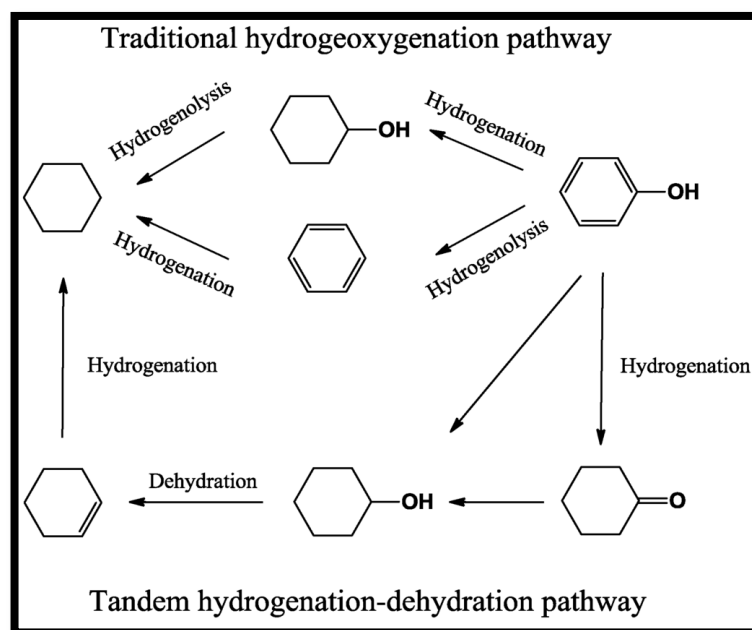


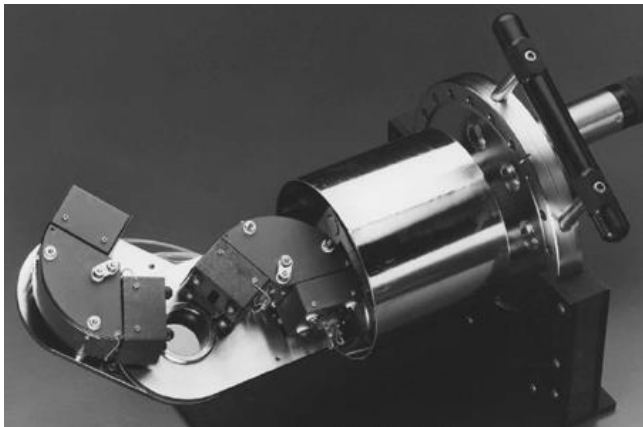

Figure 7: The traditional hydrodeoxygenation method

The rates of the four sequential reactions of phenol hydrodeoxygenation were compared over two Ni catalysts. In three hydrogenation reactions of phenol, cyclohexanone, and cyclohexene, Ni/Al₂O₃-HZSM-5 was more active than Ni/HZSM-5 due to higher Ni dispersion on Ni/Al₂O₃-HZSM-5. The Al₂O₃ binder introduced Lewis acidity that stabilized a ketone intermediate and inhibited its hydrogenation. The cyclohexanol dehydration reaction rate on Ni/HZSM-5 was slightly higher due to higher BAS concentration, and such dehydration was highly enhanced by close proximity between acid sites and metal sites where cyclohexene is irreversibly hydrogenated[2].

CHAPTER 3

METHODOLOGY AND PROJECT WORK

3.1 Materials and Equipment:

Equipment	Function
 <p>Electron Energy Loss Spectroscopy (EELS)</p>	Active side of catalyst
 <p>Fourier Transform Infrared Spectroscopy (FTIR)</p>	Organic Functional Group



Crystal structure
analysis

X-Ray Diffraction (XRD)



Surface
topography

Scanning Electron Microscopy (SEM)

Particle size
analysis



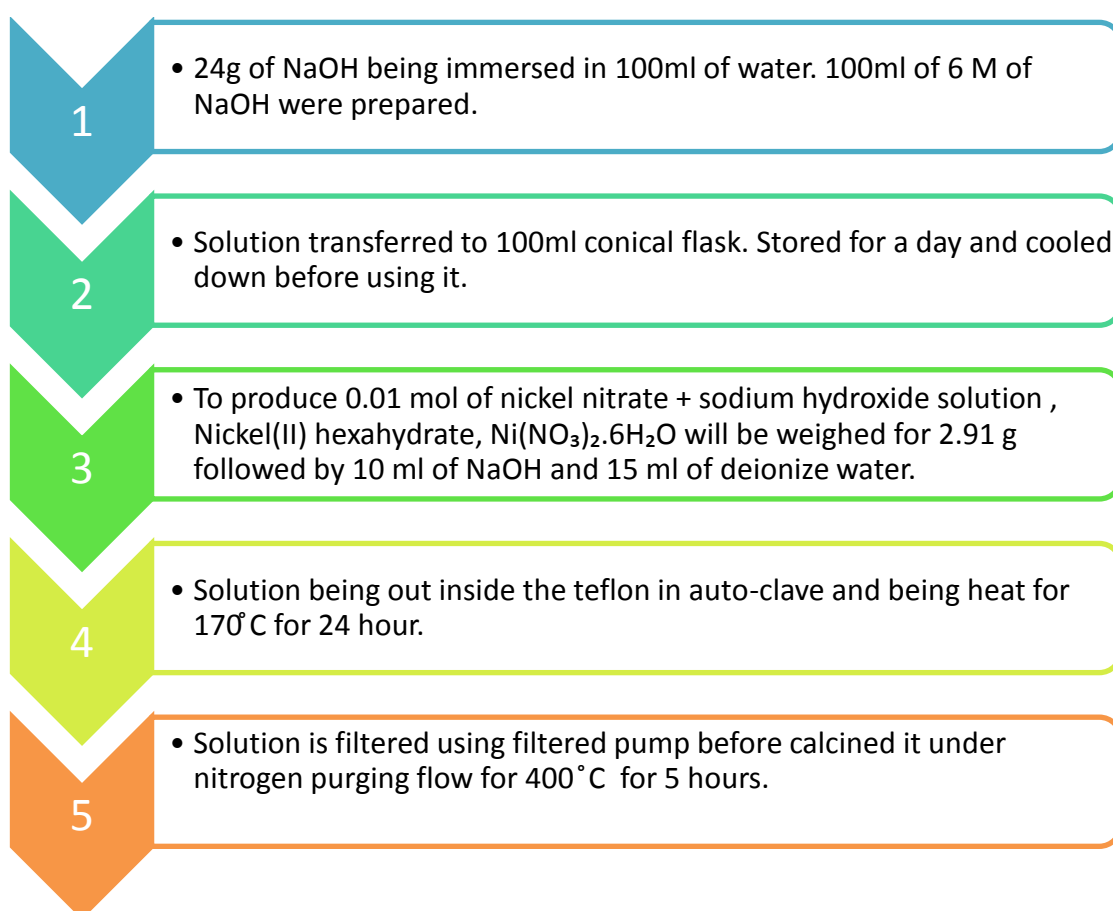
Transmission Electron Microscopy (TEM)

- ❖ Catalyst – Iron and Nickel Oxide
- ❖ Sodium hydroxide
- ❖ Batch reactor
- ❖ Deionized water
- ❖ Methanol
- ❖ Semi-batch reactor
- ❖ Thermocouple
- ❖ pH meter

3.2 Procedures

The events in this research can be alienated into three segments which are synthesis of nickel catalyst, doping and characterization of Iron (FE) over Nickel Oxide nanomaterial and biofuel production.

A. The overall processes for the synthesis of nickel catalyst are as bellows:



Timelines for FYP 1



Figure 8: Timelines for FYP I

Timelines for FYP 2

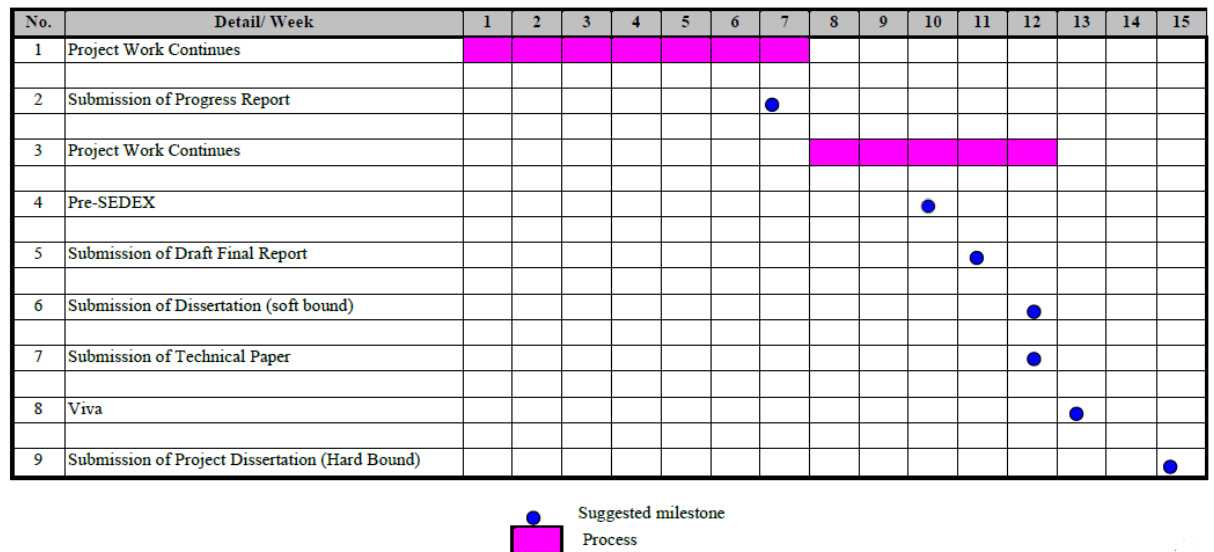


Figure 9: Timelines for FYP II

3.4 Key milestone

Several key milestones for this research project must be achieved in order to meet the objective of this project:

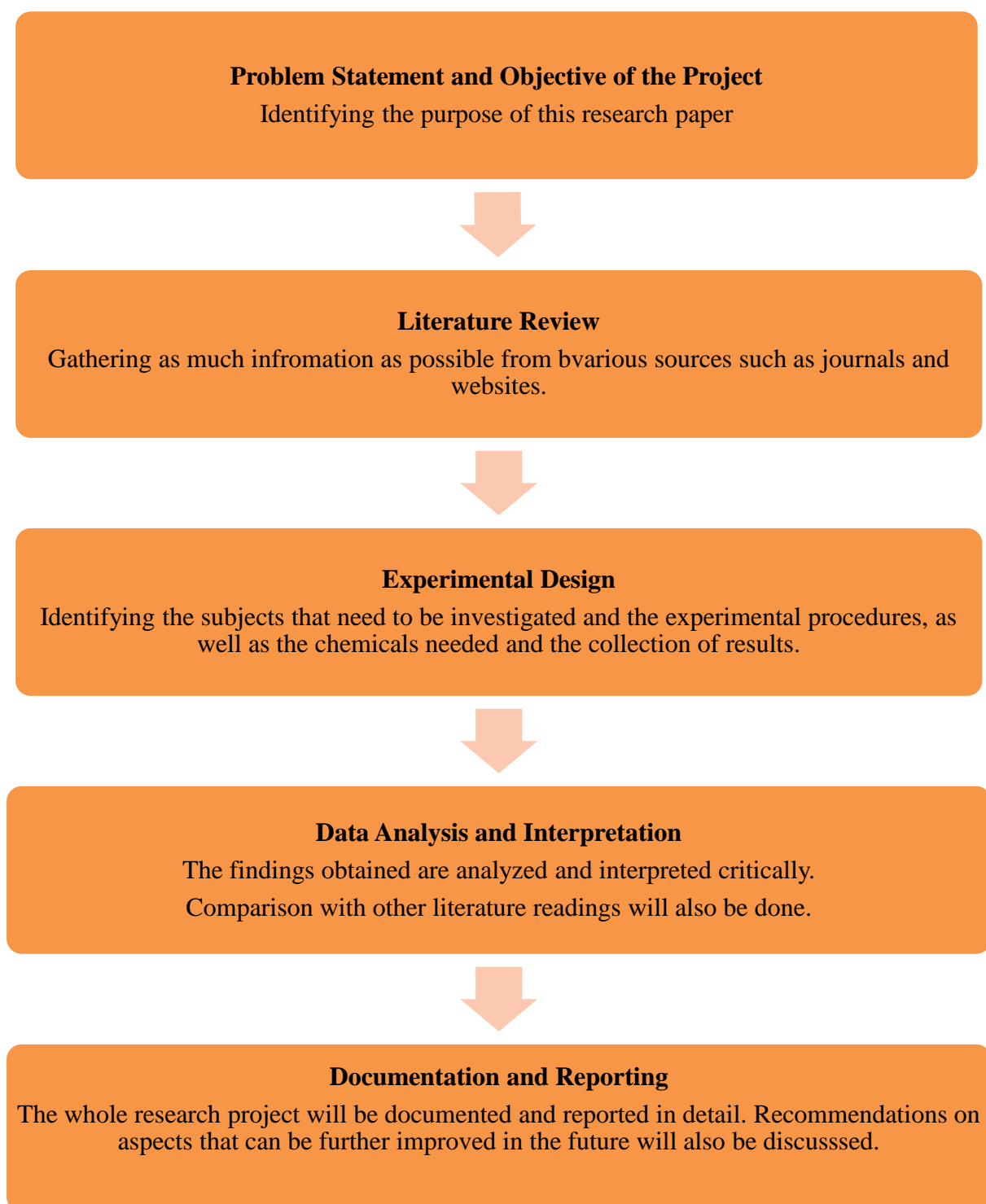


Figure 10: Key milestone

CHAPTER 4

RESULTS

1. The bases used in this experiment:

- Sodium hydroxide, NaOH
- Potassium hydroxide, KOH
- Sodium carbonate, Na₂CO₃
- Ammonia, NH₃
- Sodium Fluoride, NaF

A. Sodium hydroxide

- Prepare 100ml of 5M NaOH

1L of 5M NaOH contains 5 mol of NaOH

$$= \frac{5 \text{ mol NaOH}}{1 \text{ L solution}}$$

1 mol NaOH = 40.0g NaOH

$$?g \text{ NaOH} = 100 \text{ ml of 5M NaOH} \times \frac{1 \text{ L}}{1000 \text{ ml}} \times \frac{5 \text{ mol NaOH}}{1 \text{ L solution}} \times$$

$$\frac{40.0 \text{ g NaOH}}{1 \text{ mol NaOH}}$$

$$= 20.0 \text{ g}$$

- Prepare 100ml of 4M NaOH

1L of 4M NaOH contains 4 mol of NaOH

$$\frac{4 \text{ mol NaOH}}{1 \text{ L solution}}$$

1 mol NaOH = 40.0g NaOH

$$?g \text{ NaOH} = 100 \text{ ml of 4M NaOH} \times \frac{1 \text{ L}}{1000 \text{ ml}} \times \frac{4 \text{ mol NaOH}}{1 \text{ L solution}} \times$$

$$\frac{40.0 \text{ g NaOH}}{1 \text{ mol NaOH}}$$

$$= 16.0 \text{ g}$$

- Prepare 100ml of 2M NaOH

1L of 2M NaOH contains 2 mol of NaOH

$$\frac{2 \text{ mol NaOH}}{1 \text{ L solution}}$$

1 mol NaOH = 40.0g NaOH

$$?g \text{ NaOH} = 100 \text{ ml of 2M NaOH} \times \frac{1 \text{ L}}{1000 \text{ ml}} \times \frac{2 \text{ mol NaOH}}{1 \text{ L solution}} \times$$

$$\frac{40.0 \text{ g NaOH}}{1 \text{ mol NaOH}}$$

$$= 8.0 \text{ g}$$

- Prepare 100ml of 0.125M NaOH

1L of 0.125M NaOH contains 0.125 mol of NaOH

$$= \frac{0.125 \text{ mol NaOH}}{1 \text{ L solution}}$$

1 mol NaOH = 40.0g NaOH

$$\begin{aligned} ?\text{g NaOH} &= 100 \text{ ml of } 0.125\text{M NaOH} \times \frac{1\text{L}}{1000 \text{ ml}} \times \\ &\frac{0.125 \text{ mol NaOH}}{1 \text{ L solution}} \times \end{aligned}$$

$$\frac{40.0 \text{ g NaOH}}{1 \text{ mol NaOH}}$$

$$= 0.5 \text{ g}$$

B. Potassium hydroxide, KOH

- Prepare 100ml of 4M KOH

1L of 4M KOH contains 4 mol of KOH

$$= \frac{4 \text{ mol KOH}}{1 \text{ L solution}}$$

1 mol KOH = 56.11g KOH

$$?\text{g KOH} = 100 \text{ ml of } 4\text{M KOH} \times \frac{1\text{L}}{1000 \text{ ml}} \times \frac{4 \text{ mol KOH}}{1 \text{ L solution}} \times$$

$$\frac{56.11 \text{ g KOH}}{1 \text{ mol KOH}}$$

$$= 22.4 \text{ g}$$

C. Sodium carbonate, Na_2CO_3

- Prepare 100ml of 2M Na_2CO_3

1L of 2M Na_2CO_3 contains 2 mol of Na_2CO_3

$$= \frac{2 \text{ mol } \text{Na}_2\text{CO}_3}{1 \text{ L solution}}$$

1 mol Na_2CO_3 = 106g Na_2CO_3

$$\begin{aligned} ?\text{g } \text{Na}_2\text{CO}_3 &= 100 \text{ ml of 2M } \text{Na}_2\text{CO}_3 \times \frac{1 \text{ L}}{1000 \text{ ml}} \times \\ &\frac{2 \text{ mol } \text{Na}_2\text{CO}_3}{1 \text{ L solution}} \times \end{aligned}$$

$$\frac{106 \text{ g } \text{Na}_2\text{CO}_3}{1 \text{ mol } \text{Na}_2\text{CO}_3}$$

$$= 21.2 \text{ g}$$

D. Ammonia, NH_3

- Prepare 100ml of 4M NH_3

1L of 4M NH_3 contains 4 mol of NH_3

$$= \frac{4 \text{ mol } \text{NH}_3}{1 \text{ L solution}}$$

1 mol NH_3 = 17.031 g NH_3

$$?\text{g } \text{NH}_3 = 100 \text{ ml of 4M } \text{NH}_3 \times \frac{1 \text{ L}}{1000 \text{ ml}} \times \frac{4 \text{ mol } \text{NH}_3}{1 \text{ L solution}} \times$$

$$\frac{17.031 \text{ g } \text{NH}_3}{1 \text{ mol } \text{NH}_3}$$

$$= 6.8 \text{ g}$$

E. Sodium Fluoride, NaF

- Prepare 100ml of 4M NaF

1L of 4M NaF contains 4 mol of NaF

$$= \frac{4 \text{ mol NaF}}{1 \text{ L solution}}$$

1 mol NaF = 41.99 g NaF

$$? \text{ g NaF} = 100 \text{ ml of 4M NaF} \times \frac{1 \text{ L}}{1000 \text{ ml}} \times \frac{4 \text{ mol NaF}}{1 \text{ L solution}} \times$$

$$\frac{41.99 \text{ g NaF}}{1 \text{ mol NaF}}$$

$$= 16.796 \text{ g}$$

2. pH value of the bases

The Table 1 below shows the pH value obtained for each bases before preparing the nickel oxide catalyst. It has been found that the lower the pH value of a base the better it is, but it is not applicable for some of the bases. For example the bases with one of the lowest pH values are the 2M NaF and this base did not show any effects on the nickel oxide catalyst since it was even hard for it to be dissolved in the distilled water and also deionized water. The ideal base to be identified was the 2M of KOH with the pH value of 10.5 and also the 2M of Na₂CO₃ with the pH value of 11.1.

Types of base	pH value
5 M of NaOH	11.7
4 M of NaOH	11.1
2 M of NaOH	10.5
0.125 M of NaOH	10.2
2M of NaF	8.7
2M of NH ₃	12
2M of Na ₂ CO ₃	11.1
2M of KOH	10.4

Table 2: The pH values of the selected bases with different molar.

Besides, as you can picture in Figure 4, the bases are arranged in a descending order from the best base to be used to the lowest base to be used. The best base to be used is the 0.125M of NaOH followed by 2M of KOH, 2M of NaOH, 4M of NaOH, 2M Na_2CO_3 , 5M of NaOH and 2M of NH_3 . This is chosen based on few reasons just as the structure of the nickel oxide catalyst, the Raman results, the surface area of the catalyst, XRD result and also the EELS result.

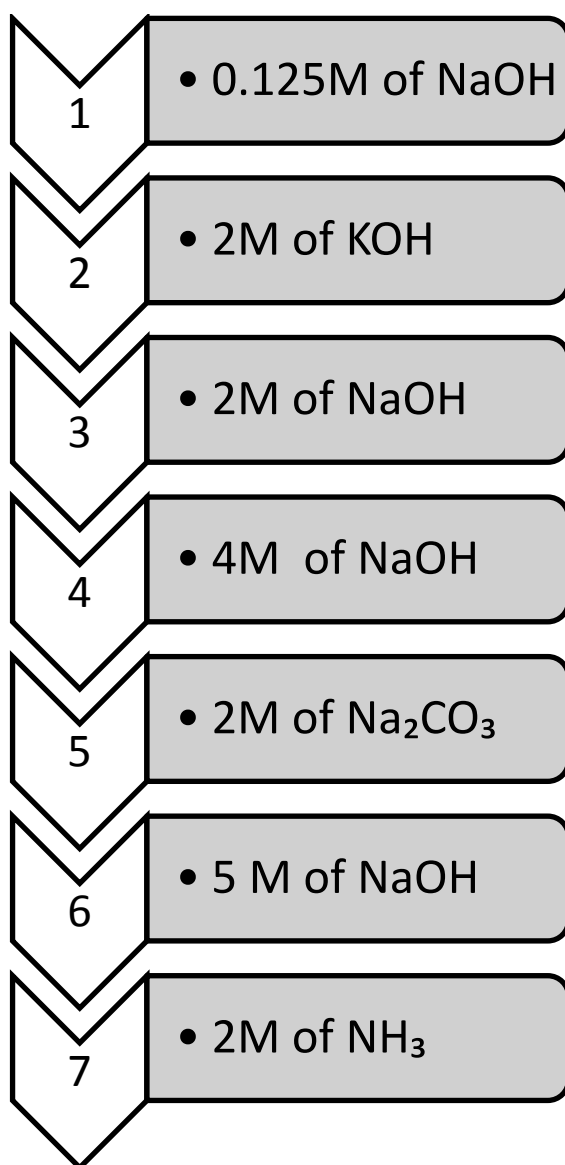
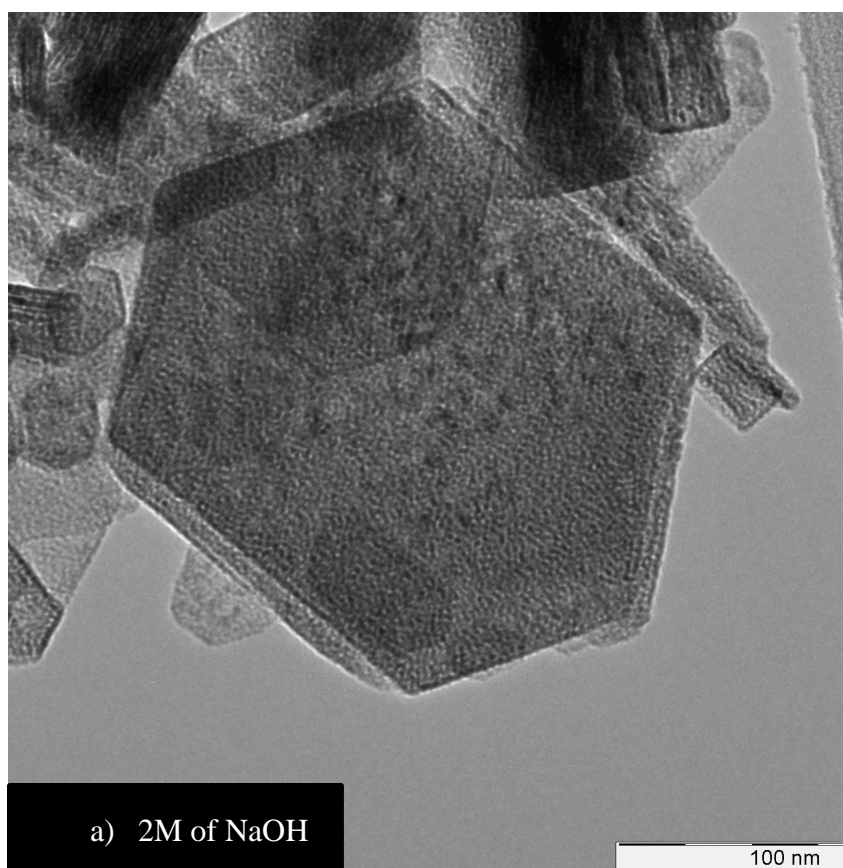
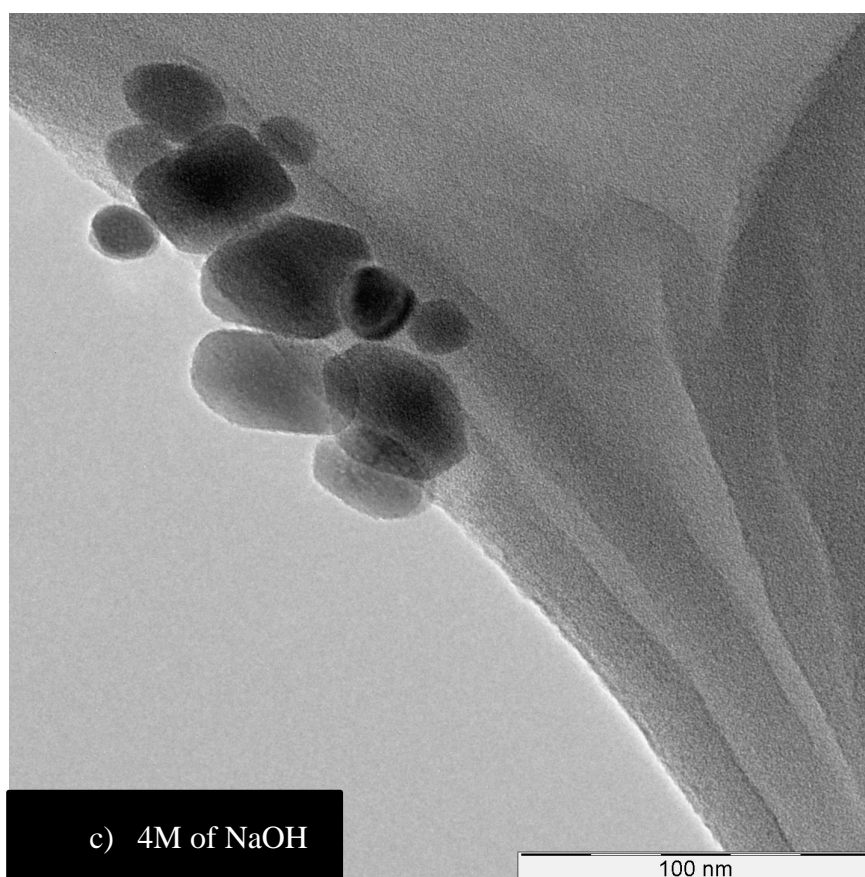
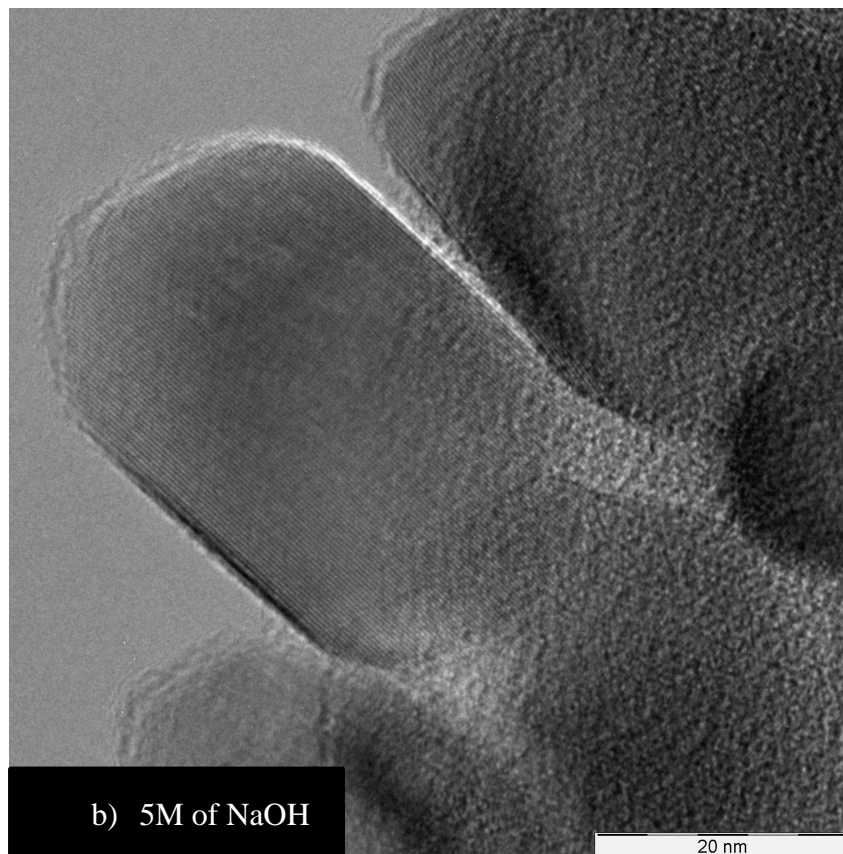


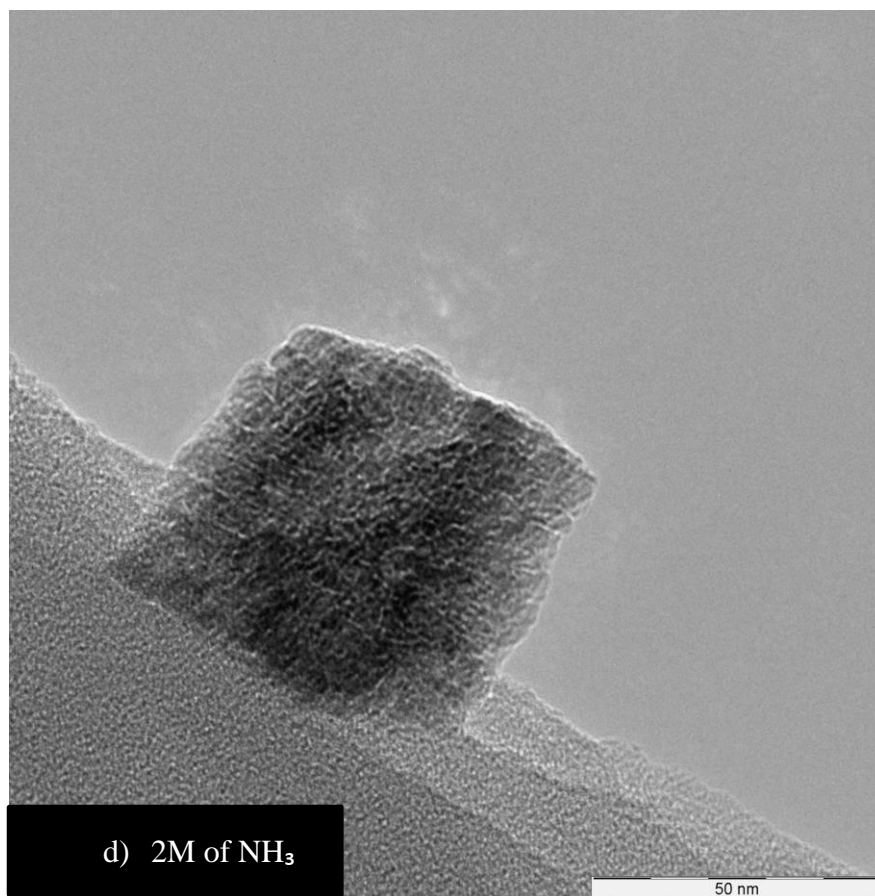
Figure 11: The descending order of the base reactivity.

3. Results from TEM

As you can see the images in Figure 5 and 6, the base reactivity does affect the structure of the nickel oxide catalyst. The lower the pH values of the base the better the structure of the nickel oxide catalyst. It shows that it has a better surface area. The structures of the nickel oxides can be seen in Figure 5 and 6. In Figure 5 (a): it shows hexagonal shaped structure catalyst, (b): shows the cuboid structure shaped catalyst, (c): shows the cubic shaped structure catalyst, (d): shows the cubic shaped structure catalyst, (e): shows the curved hexagonal shaped structure catalyst, (f): shows the mixture of long rod and hexagonal shaped structure catalyst and in Figure 6 (a): it shows the pentagon shaped structure catalyst.







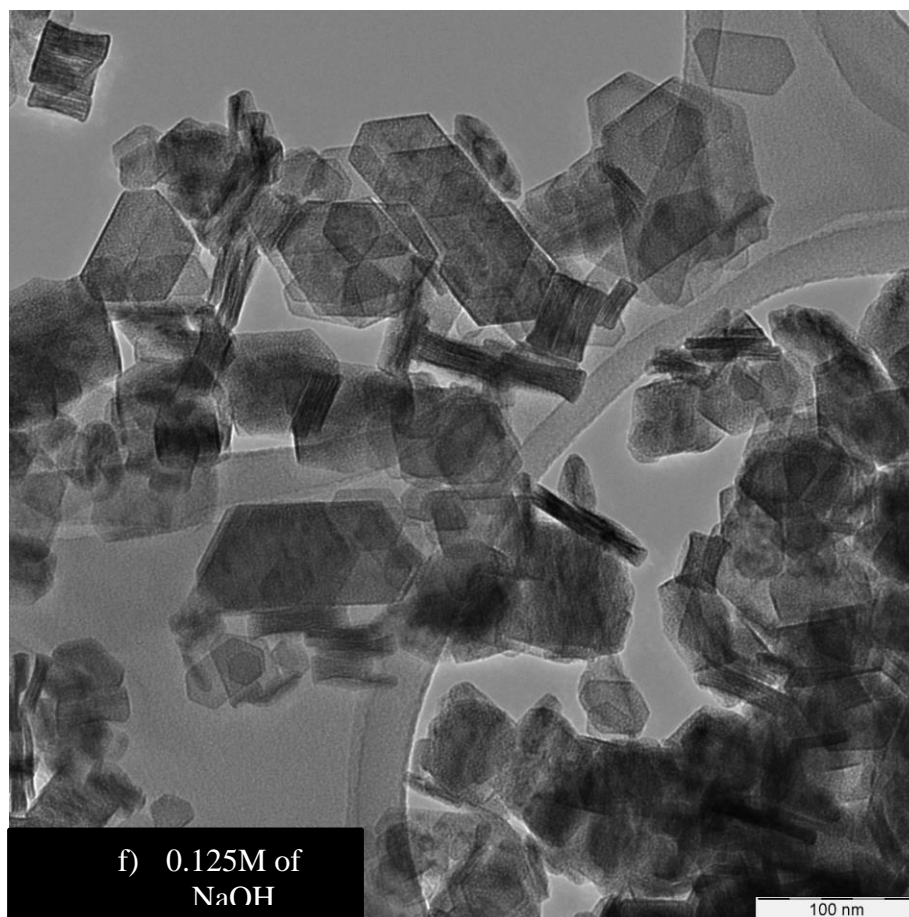
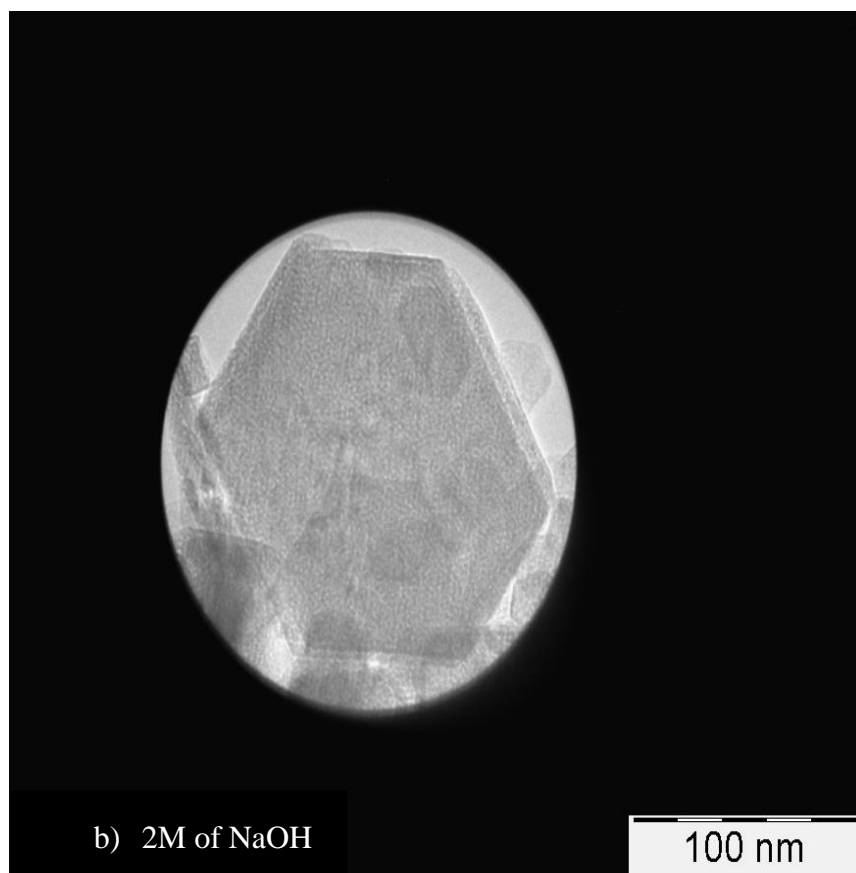
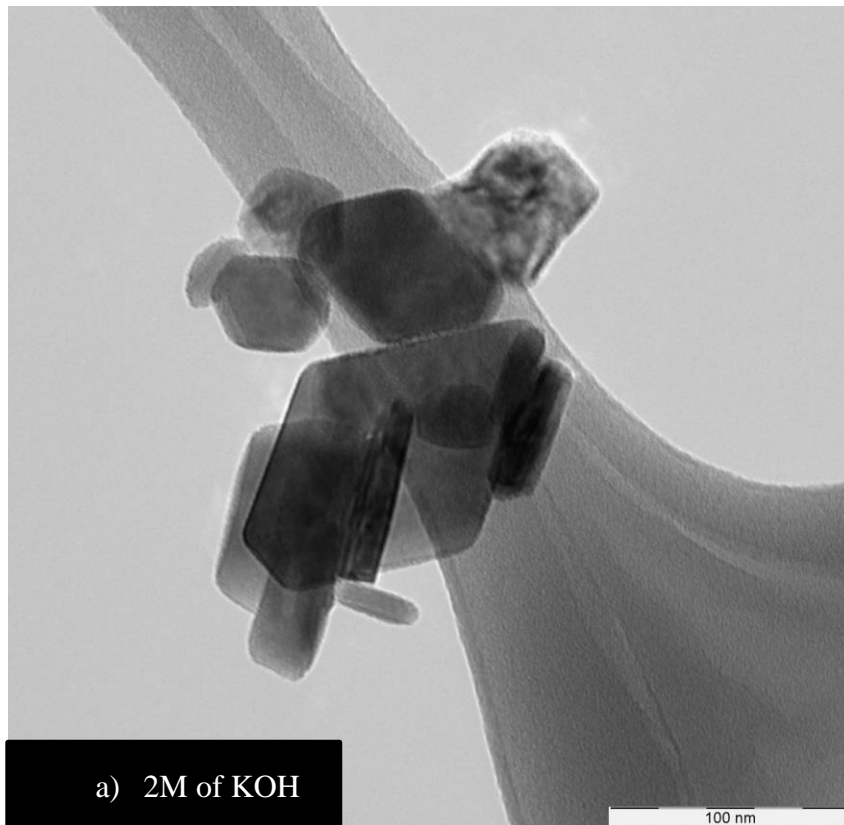
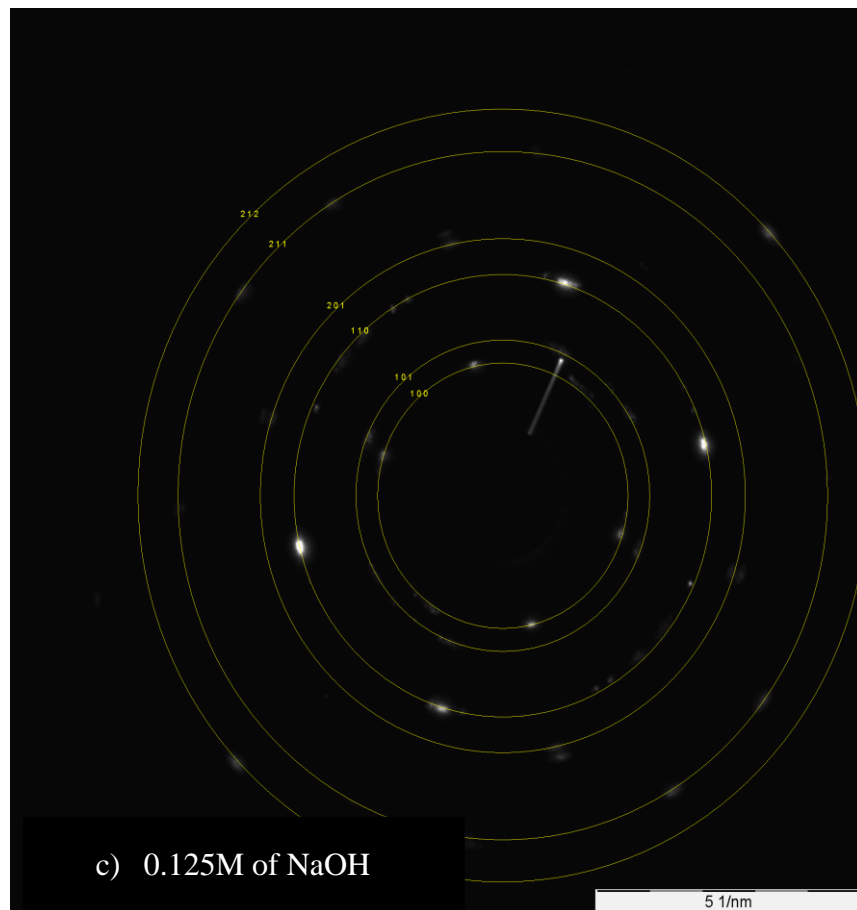


Figure 12: Different structures of nickel oxide catalyst using TEM





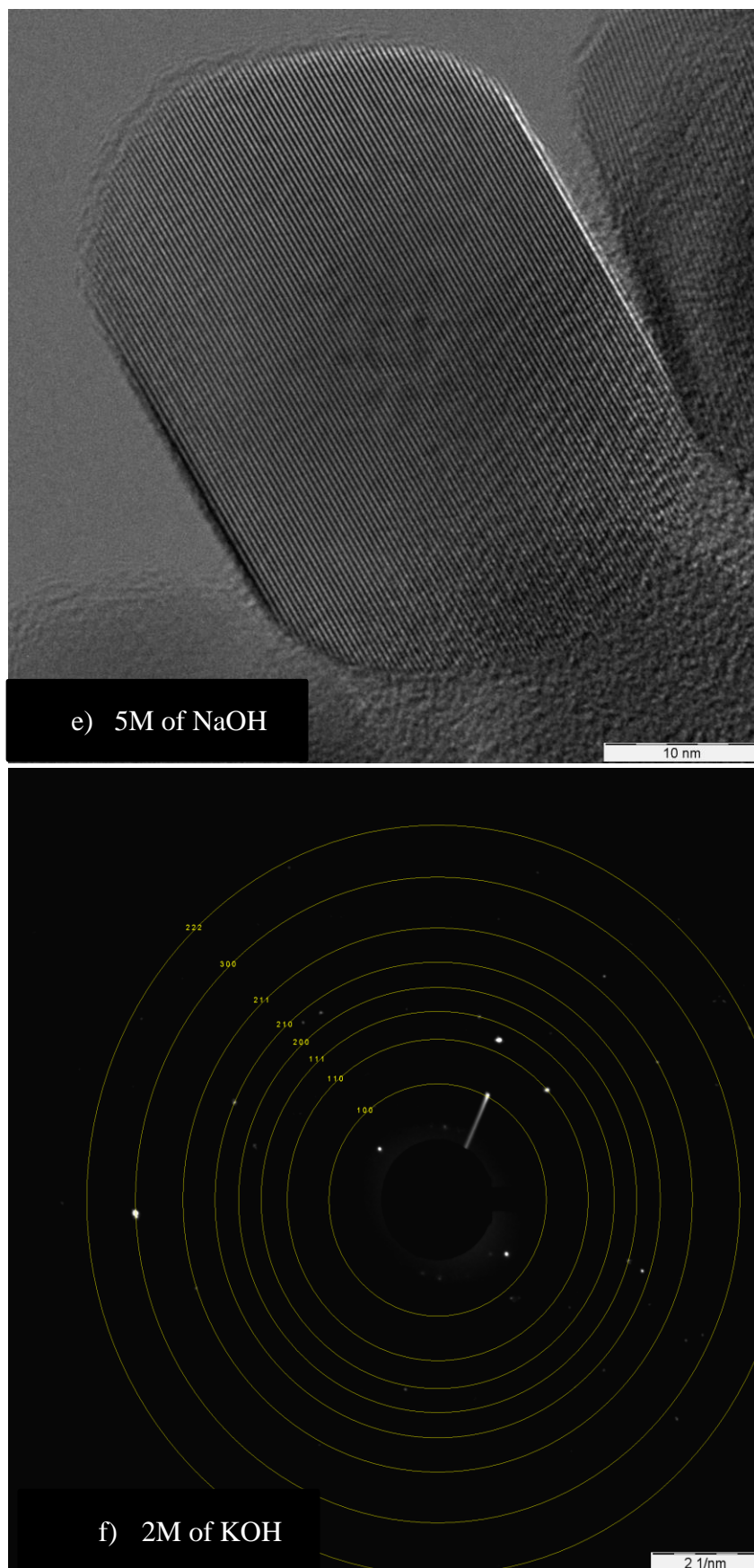
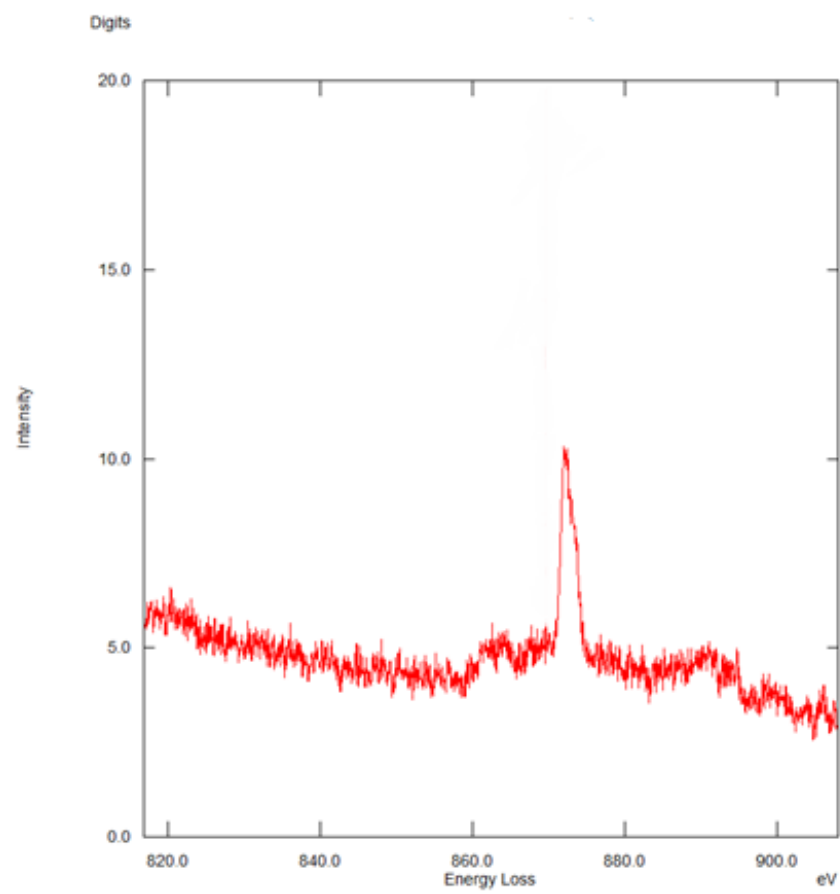


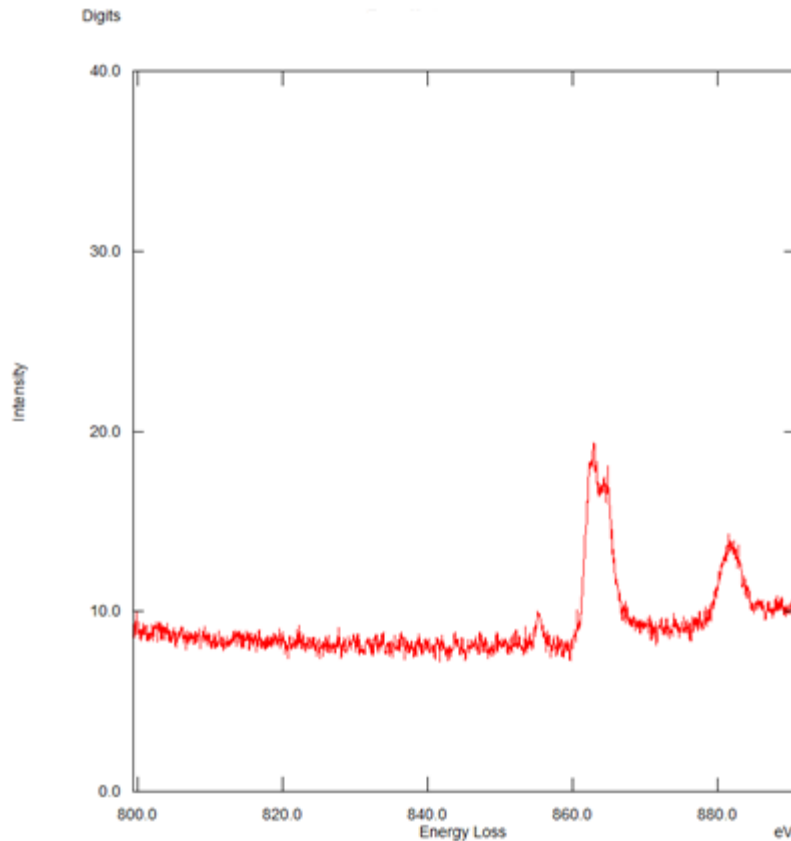
Figure 13: The diffraction rings of nickel oxide catalyst

Figure 13 (b) and (d) shows the detailed and focused of 2M of NaOH and also 4M of NaOH using TEM 'Transmission Electron Microscopy'. Figure 13 (c) and (f) shows the diffraction rings for the nickel oxide catalyst with the base of 0.125M of NaOH and also 2M of KOH.

4. Results from EELS



(a) EELS result for 0.125M of NaOH



(b) EELS result for 0.125M of NaOH

Figure 14: EELS result

EELS which also known as ‘electron energy loss spectroscopy’ is an equipment used to a contracted array of kinetic energies which also known to be visible to a ray of electrons. In this research, electron spectrometer is used to calculate the volume of energy loss. As you can in Figure 14 (a) the energy loss occurs in the 870 eV at an intensity of 10 compared to the Figure 9 (b) which occurs at 2 peaks at 856 eV at an intensity of 20 and a small peak at 860 eV at an intensity of 15. The EELS of Figure 14 (a) which is the nickel oxide with the NaOH bases shows a better graph compared to the other one. Both show that nickel and oxygen are present.

5. Results from SEM

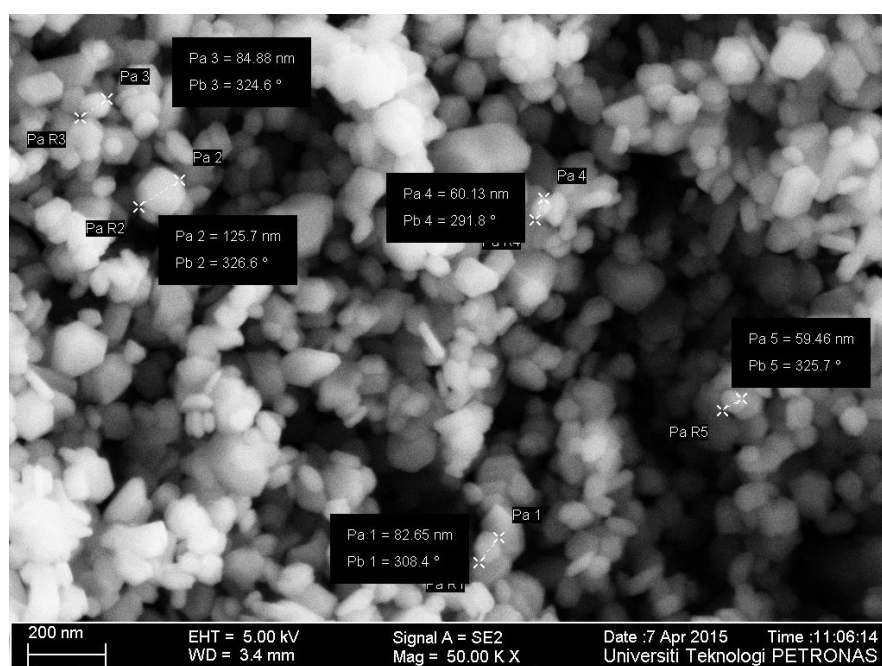


Figure 15: SEM result of 2M of KOH nickel oxide catalyst

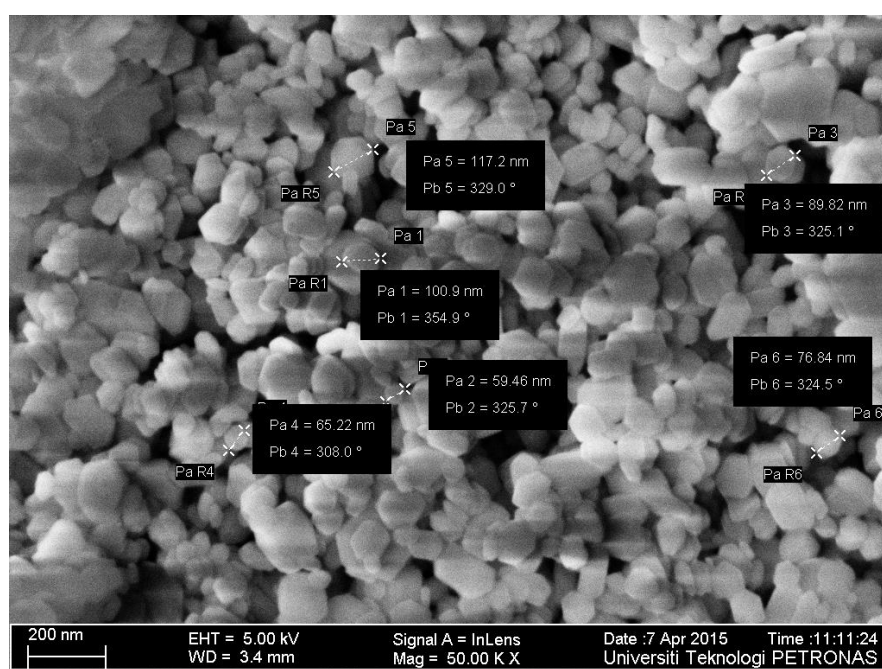
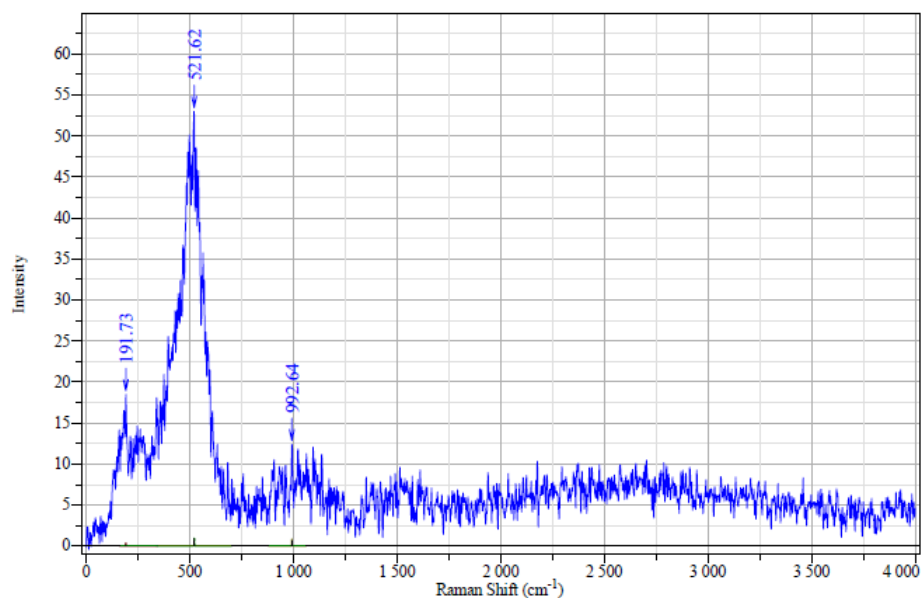


Figure 16: SEM result of 0.125M of NaOH of nickel oxide catalyst

Figure 15 and 16 shows the SEM results of 2M of KOH nickel oxide catalyst and 0.125M of NaOH of nickel oxide catalyst.

6. Results from RAMAN

a) Raman result for 0.125M NaOH



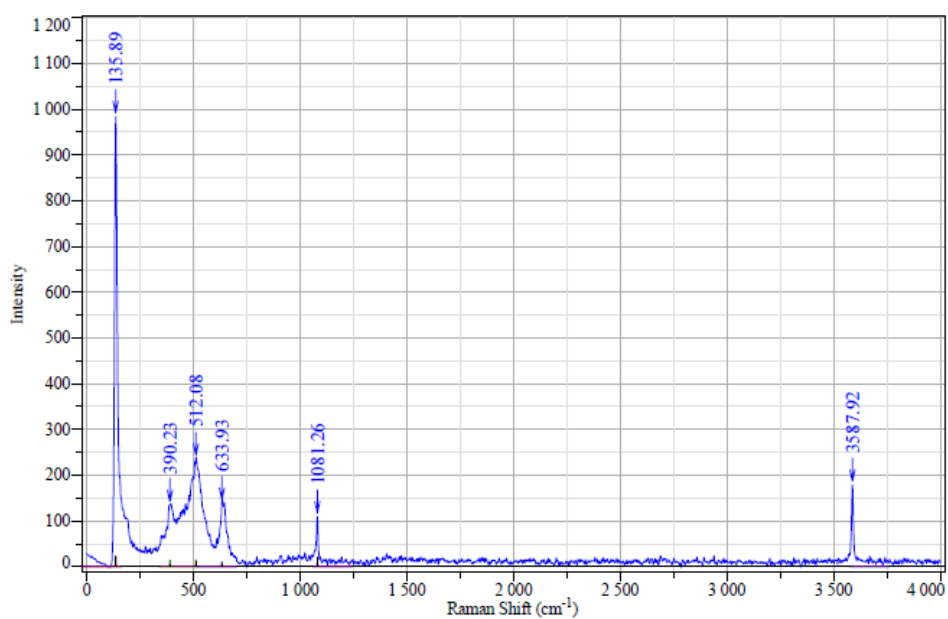
Exposition	1	Slit	100
Accumulation	1	Operator	Hasbullah
Laser	514.53	Sample	2M NaOH
Spectro	Multi	Remark	
Hole	1000	Power	

HORIBAJOBIN YVON

Figure 17: Raman result for 0.125M NaOH

The highest peak of this concentration is at 521.62 cm^{-1} at the intensity of 52.5.

b) Raman result for 4M NaOH



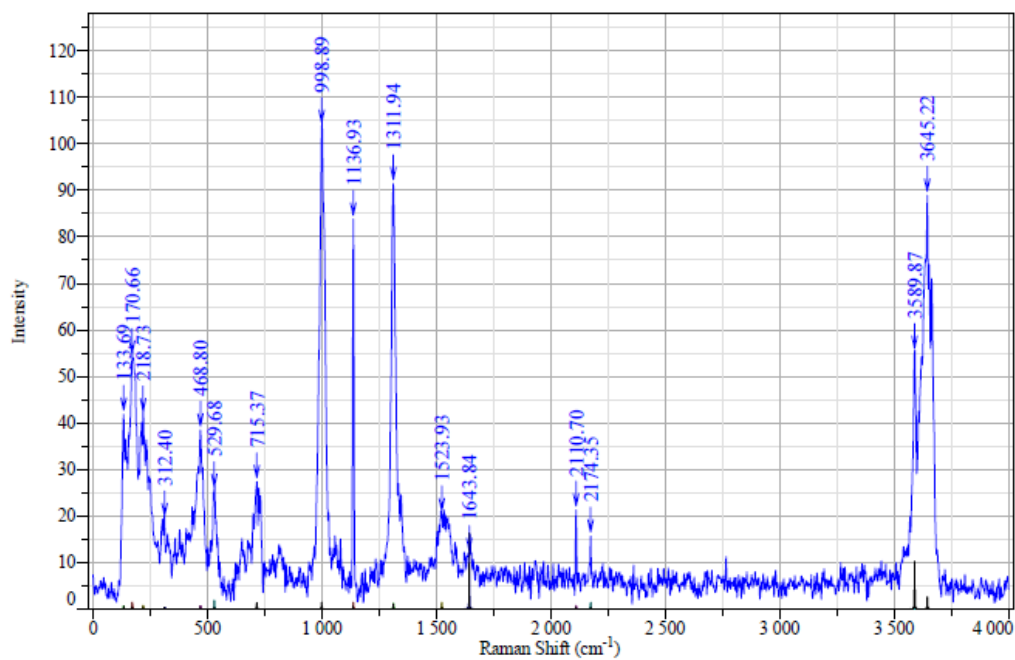
Exposition	1	Slit	100
Accumulation	1	Operator	Hasbullah
Laser	514.53	Sample	No label
Spectro	Multi	Remark	
Hole	1000	Power	

HORIBAJOBIN YVON

Figure 18: Raman result for 4M NaOH

The highest peak of this concentration is at 135.89 cm^{-1} at the intensity of 98.

c) Raman result for 2M KOH



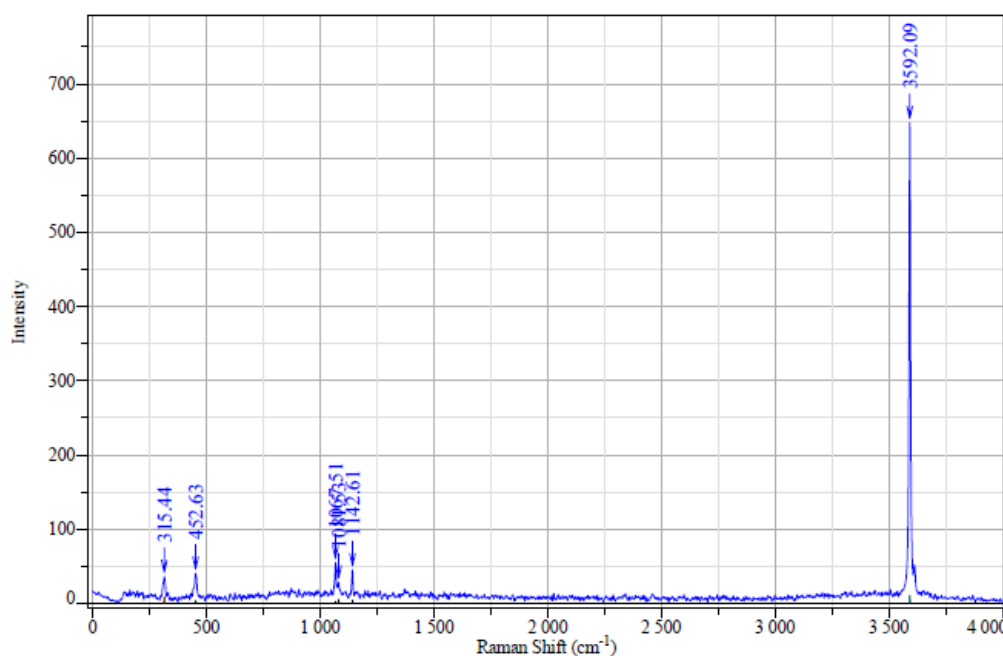
Exposition	1	Slit	100
Accumulation	1	Operator	Hasbullah
Laser	514.53	Sample	4M KOH
Spectro	Multi	Remark	
Hole	1000	Power	

HORIBAJOBIN

Figure 19: Raman result for 2M KOH

The highest peak of this concentration is at 3645.22 cm⁻¹ at the intensity of 90.

d) Raman result for 2M NaOH



Exposition	1	Slit	100
Accumulation	1	Operator	Hasbullah
Laser	514.53	Sample	2M sodium carbonate
Spectro	Multi	Remark	
Hole	1000	Power	

HORIBAJOBIN

Figure 20: Raman result for 2M NaOH

The highest peak of this concentration is at 3592.09 cm⁻¹ at the intensity of 650.

e) **Raman comparisons with different bases**

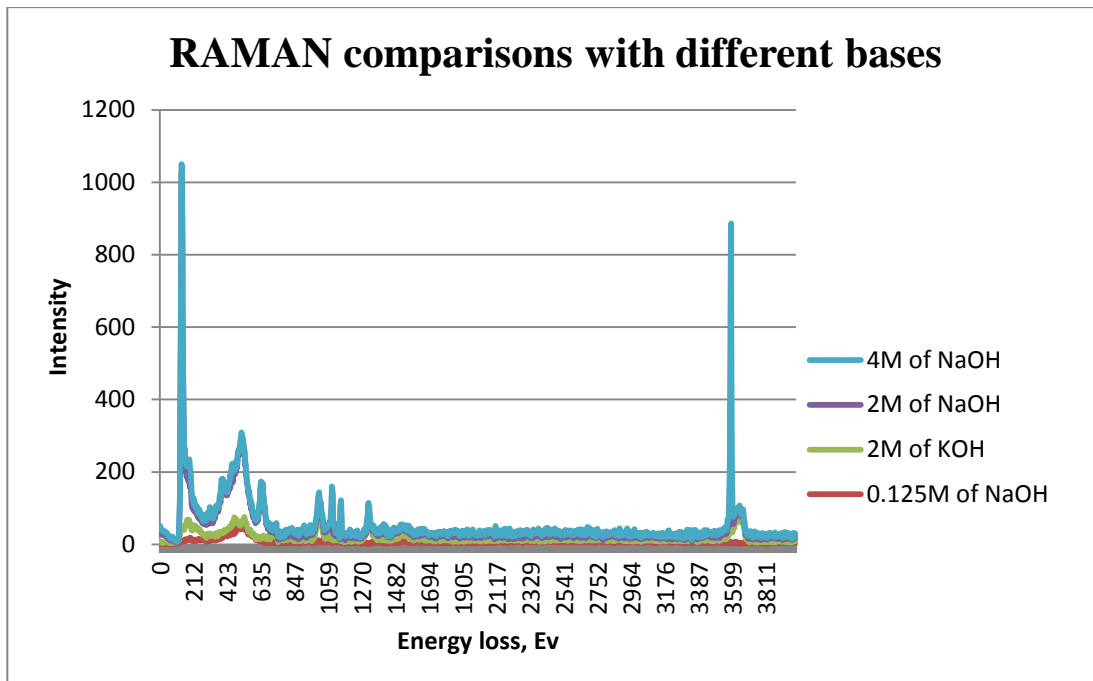


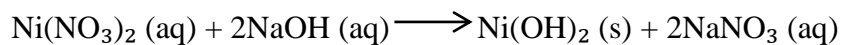
Figure 21: Comparisons of RAMAN results of four bases

Figure 11 (b) nickel oxide with the base of 2M of KOH, the highest peak of this concentration is at 3645.22 cm^{-1} at the intensity of 90. Figure 11 (c) nickel oxide with the base of 4M of NaOH, the highest peak of this concentration is at 135.89 cm^{-1} at the intensity of 98. Lastly, Figure 11 (d) nickel oxide with the base of 2M of NaOH, the highest peak of this concentration is at 3592.09 cm^{-1} at the intensity of 650.

Figure 12 shows the Raman comparisons of four bases which are the nickel oxide with the base of 0.125M of NaOH, nickel oxide with the base of 2M of KOH, nickel oxide with the base of 4M of NaOH, and nickel oxide with the base of 2M of NaOH. From the comparison we can conclude that 0.125M of NaOH has the best result followed by 2M of KOH, then 2M of NaOH and lastly 4M of NaOH.

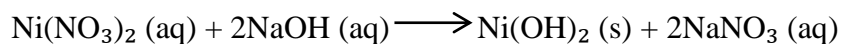
7. Rate of reaction

a. 5M of NaOH



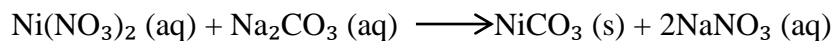
$$\begin{aligned}\text{Rate} &= -\left(\frac{\Delta \text{Ni}(\text{NO}_3)_2}{\Delta t}\right) \\ &= -\frac{1}{2} \left(\frac{\Delta \text{NaOH}}{\Delta t}\right) \\ &= -\frac{1}{2} \left(\frac{5M (\text{pH:11.7})}{24 \text{ hrs}}\right) \\ &= -0.0417\end{aligned}$$

b. 4M of NaOH



$$\begin{aligned}\text{Rate} &= -\left(\frac{\Delta \text{Ni}(\text{NO}_3)_2}{\Delta t}\right) \\ &= -\frac{1}{2} \left(\frac{\Delta \text{NaOH}}{\Delta t}\right) \\ &= -\frac{1}{2} \left(\frac{4M (\text{pH:11.1})}{24 \text{ hrs}}\right) \\ &= -0,1042\end{aligned}$$

c. 2M of NaOH

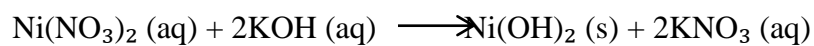


$$\begin{aligned}\text{Rate} &= -\left(\frac{\Delta \text{Ni}(\text{NO}_3)_2}{\Delta t}\right) \\ &= -\frac{1}{2} \left(\frac{\Delta \text{NaOH}}{\Delta t}\right)\end{aligned}$$

$$= -\frac{1}{2} \left(\frac{2M \text{ (pH:10.5)}}{24 \text{ hrs}} \right)$$

$$= -0.1177$$

d. 0.125M of NaOH



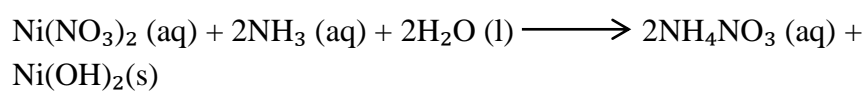
$$\text{Rate} = -\left(\frac{\Delta \text{Ni(NO}_3)_2}{\Delta t} \right)$$

$$= -\frac{1}{2} \left(\frac{\Delta \text{NaOH}}{\Delta t} \right)$$

$$= -\frac{1}{2} \left(\frac{0.125M \text{ (pH:10.2)}}{24 \text{ hrs}} \right)$$

$$= -0.1608$$

e. 2M of NH₃



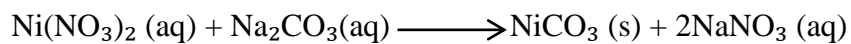
$$\text{Rate} = -\left(\frac{\Delta \text{Ni(NO}_3)_2}{\Delta t} \right)$$

$$= -\frac{1}{2} \left(\frac{\Delta \text{NH}_3}{\Delta t} \right)$$

$$= -\frac{1}{2} \left(\frac{2M \text{ (pH:12)}}{24 \text{ hrs}} \right)$$

$$= -0.0026$$

f. 2M of Na₂CO₃



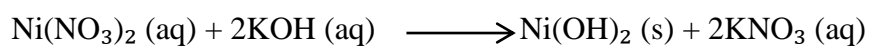
$$\text{Rate} = -\left(\frac{\Delta \text{Ni}(\text{NO}_3)_2}{\Delta t}\right)$$

$$= -\left(\frac{\Delta \text{Na}_2\text{CO}_3}{\Delta t}\right)$$

$$= -\frac{1}{2} \left(\frac{0.125 \text{ M (pH:10.2)}}{24 \text{ hrs}} \right)$$

$$= -0.0830$$

g. 2M of KOH



$$\text{Rate} = -\left(\frac{\Delta \text{Ni}(\text{NO}_3)_2}{\Delta t}\right)$$

$$= -\frac{1}{2} \left(\frac{\Delta \text{NaOH}}{\Delta t} \right)$$

$$= -\frac{1}{2} \left(\frac{2 \text{ M (pH:10.4)}}{24 \text{ hrs}} \right)$$

$$= -0.1382$$

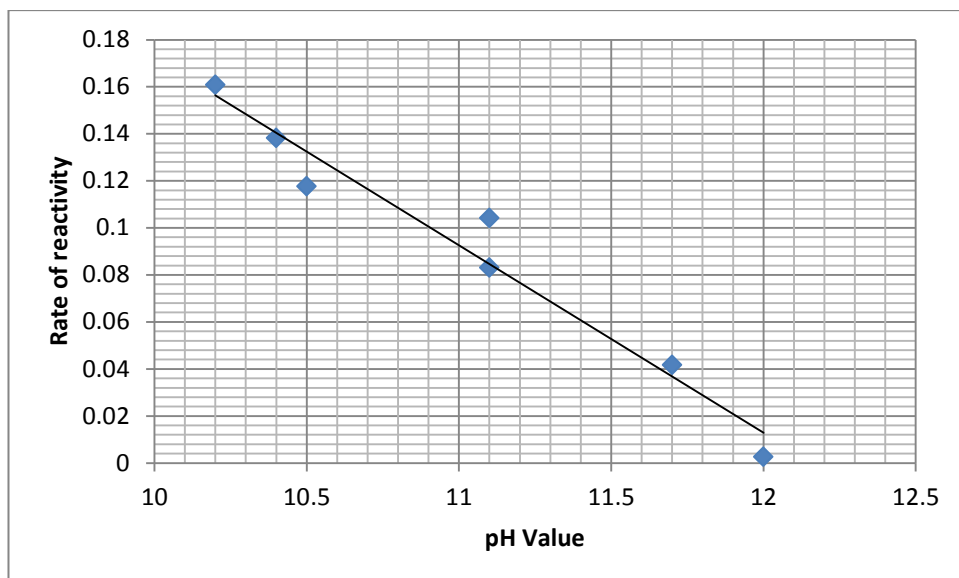


Figure 22: Graph of rate of reactivity versus pH values

The graph below shows the graph of rate of reactivity versus the pH values of the bases. As you can see in the graph as the pH value increases the rate of reactivity decreases. This proves that the pH values do have effect the rate of reactivity as told in the beginning of the research paper. It is also proven with the structure obtained from the TEM structures.

8. Results from XRD

The XRD (X-ray diffraction) pattern of the green nickel oxide of 0.125M of NaOH obtained from the calcination is pictured in Figure 3. The study from the pattern shows that it is a classic alpha-type nickel oxide in their powder form. The diffraction crests where large and all it shows that it fits to $\text{NiO} \cdot 6\text{H}_2\text{O}$. They are said to be in minor grain structure or micro -structural alteration. This is because of the wide crests and the patterns from the analysis shows that it has orientationally tangled films with an indication of “saw-tooth” pattern.

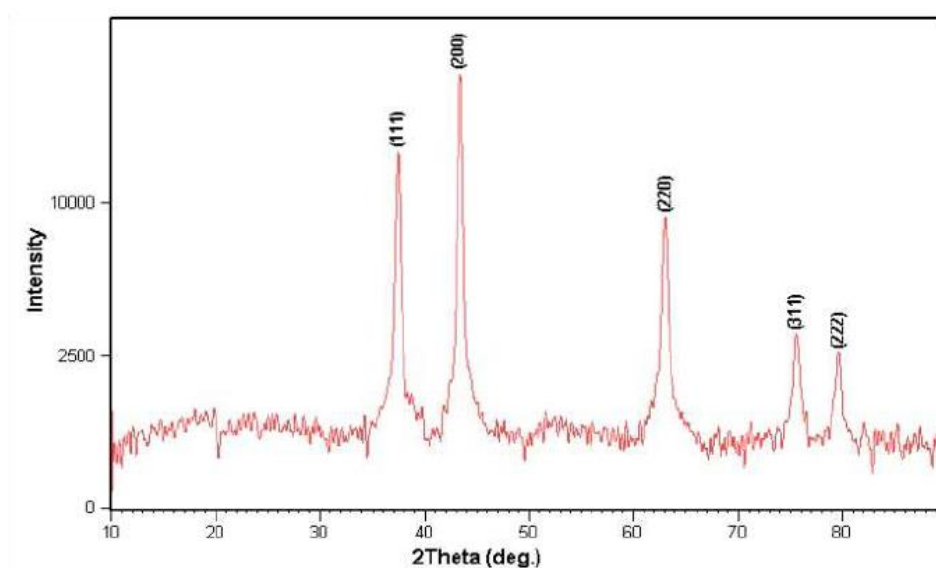


Figure 23: The XRD pattern of the nickel oxide of 0.125M of NaOH.

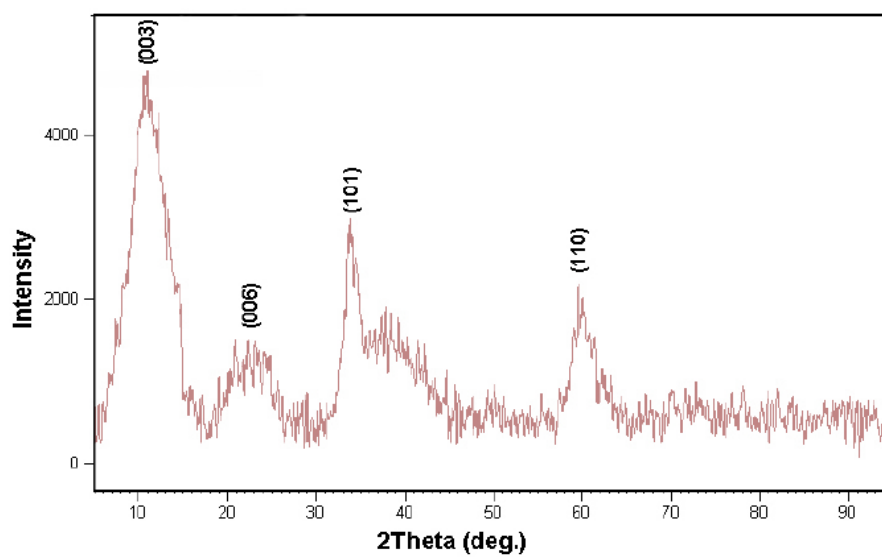


Figure 24: The XRD pattern of the nickel oxide of 2M of KOH.

CHAPTER 5

CONCLUSION AND RECCOMENDATION

The synthesis of Nickel nanomaterials are believed to be aiding the hydrodeoxygenation of phenol with the production of different structured nickel in this research paper. The best base to be used is the 0.125M of NaOH followed by 2M of KOH, 2M of NaOH, 4M of NaOH, 2M Na_2CO_3 , 5M of NaOH and 2M of NH_3 . This is chosen based on few reasons just as the structure of the nickel oxide catalyst, the Raman results, the surface area of the catalyst, XRD result and also the EELS result. All the objectives are aimed to be achieved and by solving the problem statement to benefit the society with a good engineering design. The rate of reaction of nickel nitrate is affected by the pH value of the bases used.

All the objectives are aimed to be achieved and by solving the problem statement to benefit the society with a good engineering design. The rate of reaction of nickel nitrate is affected by the pH value of the bases used and also their concentration.

Lastly my recommendation is to be obtaining more different structures of nickel oxide catalyst with higher surface area and also to research on a different method of producing the nickel catalyst other than hydrothermal process. Besides, to dope the nickel oxide with other transition metal.

REFERENCES

- [1] S. K. Tanneru and P. H. Steele, "Pretreating bio-oil to increase yield and reduce char during hydrodeoxygenation to produce hydrocarbons," *Fuel*, vol. 133, pp. 326–331, 2014.
- [2] C. Zhao, S. Kasakov, J. He, and J. A. Lercher, "Comparison of kinetics, activity and stability of Ni/HZSM-5 and Ni/Al₂O₃-HZSM-5 for phenol hydrodeoxygenation," *Journal of Catalysis*, vol. 296, pp. 12–23, 2012.
- [3] S. Zhang, S. Zhang, L. Song, X. Wu, and S. Fang, "Three-dimensional interconnected nickel phosphide networks with hollow microstructures and desulfurization performance," *Materials Research Bulletin*, vol. 53, pp. 158–162, 2014.
- [4] J. G. Dickinson and P. E. Savage, "Stability and activity of Pt and Ni catalysts for hydrodeoxygenation in supercritical water," *Journal of Molecular Catalysis A: Chemical*, vol. 388–389, pp. 56–65, 2014.
- [5] S. Liu, J. Jia, J. Wang, S. Liu, X. Wang, H. Song, *et al.*, "Synthesis of Fe-doped NiO nanofibers using electrospinning method and their ferromagnetic properties," *Journal of Magnetism and Magnetic Materials*, vol. 324, pp. 2070–2074, 2012.
- [6] D. Kamaludin, "An ab initio study of Fe-doped Nickel Oxide," pp. 1–22, 2006.
- [7] Y.-D. Luo, Y.-H. Lin, X. Zhang, D. Liu, Y. Shen, and C.-W. Nan, "Ferromagnetic Behaviors in Fe-Doped NiO Nanofibers Synthesized by Electrospinning Method," *Journal of Nanomaterials*, vol. 2013, pp. 1–4, 2013.
- [8] R. R. B. P Mallick; Chandana, "Structural and magnetic properties of Fe doped NiO," *Indian J. Phys.* 83 (4) 517–523 (2009), 2009.
- [9] S. Jin, Z. Xiao, C. Li, X. Chen, L. Wang, J. Xing, *et al.*, "Catalytic hydrodeoxygenation of anisole as lignin model compound over supported nickel catalysts," *Catalysis Today*, vol. 234, pp. 125–132, 2014.
- [10] B. Güvenatam, O. Kurşun, E. H. J. Heeres, E. A. Pidko, and E. J. M. Hensen, "Hydrodeoxygenation of mono- and dimeric lignin model compounds on noble metal catalysts," *Catalysis Today*, vol. 233, pp. 83–91, 2014.

- [11] T. V. Choudhary and C. B. Phillips, "Renewable fuels via catalytic hydrodeoxygenation," *Applied Catalysis A: General*, vol. 397, pp. 1–12, 4/30/ 2011.
- [12] O. B. Ayodele, O. S. Togunwa, H. F. Abbas, and W. M. A. W. Daud, "Preparation and characterization of alumina supported nickel-oxalate catalyst for the hydrodeoxygenation of oleic acid into normal and iso-octadecane biofuel," *Energy Conversion and Management*, pp. 1–7, 2014.
- [13] Peters, J. F., Iribarren, D., & Dufour, J. (2014). Simulation and life cycle assessment of biofuel production via fast pyrolysis and hydrouprgrading. *Fuel*.
- [14] Yoon, Y., Rousseau, R., Weber, R. S., Mei, D., & Lercher, J. A. (2014). First-Principles Study of Phenol Hydrogenation on Pt and Ni Catalysts in Aqueous Phase. *Journal of the American Chemical Society*, 136(29), 10287–10298.
- [15] Boullosa-Eiras, S., Lødeng, R., Bergem, H., Stöcker, M., Hannevold, L., & Blekkan, E. A. (2014). Catalytic hydrodeoxygenation (HDO) of phenol over supported molybdenum carbide, nitride, phosphide and oxide catalysts. *Catalysis Today*, 223, 44–53.
- [16] Palla, Venkata Chandra Sekhar, Debaprasad Shee, and Sunil K. Maity. "Kinetics of hydrodeoxygenation of octanol over supported nickel catalysts: a mechanistic study." *RSC Advances* 4.78 (2014): 41612–41621.
- [17] Adjaye, J.D., Bakhshi, N.N., 1995. Production of hydrocarbons by catalytic upgrading of a fast pyrolysis bio-oil. Part II: Comparative catalyst performance and reaction pathways. *Fuel Processing Technology* 45, 185–202.
- [18] Brems, A., Dewil, R., Baeyens, J., Seville, J.P.K. Prayogo, C., Bending, G., 2011. The future of biomass pyrolysis in the production of value-added products. In: *Proceedings of the SDEWES Conference*, Dubrovnik, September 26–29.
- [19] S. Manna, A. K. Deb, J. Jagannath, and S. K. De, "Synthesis and room temperature ferromagnetism in Fe doped NiO nanorods," *Journal of Physical Chemistry C*, vol. 112, no. 29, pp.10659–10662, 2008.
- [20] W. Yan, W. Weng, G. Zhang et al., "Structures and magnetic properties of (Fe, Li)-codoped NiO thin films," *Applied Physics Letters*, vol. 92, no. 5, Article ID 052508, 3 pages, 2008.
- [21] Y. H. Lin, J. Wang, J. Cai et al., "Ferromagnetism and electrical transport in Fe-doped NiO," *Physical Review B*, vol. 73, no. 19, 4 pages, 2006.
- [22] Y. H. Lin, R. J. Zhao, C. W. Nan, and M. H. Ying, "Enhancement of ferromagnetic properties of NiO:Fe thin film by Li doping," *Applied Physics Letters*, vol. 89, no. 20, 3 pages, 2006.

- [23] Bridgwater, A. V. (2012). Review of fast pyrolysis of biomass and product upgrading. *Biomass and Bioenergy*, 38, 68-94.
- [24] S. Fernando, S. Adhikari, C. Chandrapal and N. Murali, *Energy Fuels*, 2006, 20, 1727–1737.
- [25] Solantausta, Y., Oasmaa, A., Sipila, K., Lindfors, C., Lehto, J., Autio, J and Heiskanen, J. (2011). Bio-oil production from biomass: steps toward demonstration. *Energy & Fuels*, 26(1), 233-240.
- [26] Zhao, C.; Lercher, J. A. Upgrading pyrolysis oil over Ni/HZSM-5 by cascade reactions. *Angew. Chem., Int. Ed.* 2012, 51, 5935–5940.
- [27] Echeandia, S.; Arias, P. L.; Barrio, V. L.; Pawelec, B.; Fierro, J. L. G. Synergy effect in the HDO of phenol over Ni–W catalysts supported on active carbon: Effect of tungsten precursors. *Appl. Catal., B* 2010, 101, 1–12.
- [28] Naik, S. N., Goud, V. V., Rout, P. K., & Dalai, A. K. (2010). Production of first and second generation biofuels: a comprehensive review. *Renewable and Sustainable Energy Reviews*, 14(2), 578-597.
- [29] Li, X., Gunawan, R., Wang, Y., Chaiwat, W., Hu, X., Gholizadeh, M., & Li, C. Z. (2014). Upgrading of bio-oil into advanced biofuels and chemicals. Part III. Changes in aromatic structure and coke forming propensity during the catalytic hydrotreatment of a fast pyrolysis bio-oil with Pd/C catalyst. *Fuel*, 116, 642-649.